nature microbiology

Article

https://doi.org/10.1038/s41564-024-01823-6

Vibrio cholerae virulence is blocked by chitosan oligosaccharide-mediated inhibition of ChsR activity

Received: 27 July 2023

Accepted: 4 September 2024

Published online: 16 October 2024

Check for updates

Yutao Liu[1,5], Jialin Wu[2,5], Ruiying Liu[1,5], Fan Li[1], Leyan Xuan[2], Qian Wang[1], Dan Li[1], XinTong Chen[1], Hao Sun[1], Xiaoya Li[1], Chen Jin[1], Di Huang[1], Linxing Li[1], Guosheng Tang[2] ✉ & Bin Liu[1,3,4] ✉

Vibrio cholerae causes cholera, an important cause of death worldwide. A fuller understanding of how virulence is regulated offers the potential for developing virulence inhibitors, regarded as efficient therapeutic alternatives for cholera treatment. Here we show using competitive infections of wild-type and mutant bacteria that the regulator of chitosan utilization, ChsR, increases *V. cholerae* virulence in vivo. Mechanistically, RNA sequencing, chromatin immunoprecipitation with sequencing and molecular biology approaches revealed that ChsR directly upregulated the expression of the virulence regulator, TcpP, which promoted expression of the cholera toxin and the toxin co-regulated pilus, in response to low O_2 levels in the small intestine. We also found that chitosan degradation products inhibit the ChsR–*tcpP* promoter interaction. Consistently, administration of chitosan oligosaccharide, particularly when delivered via sodium alginate microsphere carriers, reduced *V. cholerae* intestinal colonization and disease severity in mice by blocking the *chsR*-mediated pathway. These data reveal the potential of chitosan oligosaccharide as supplemental therapy for cholera treatment and prevention.

Vibrio cholerae is the causative agent of cholera, a severe and sometimes fatal diarrhoeal disease. The current, seventh, pandemic began in 1961. It is estimated that *V. cholerae* causes 3 to 5 million cases of cholera annually, resulting in 100,000 to 120,000 deaths every year[1–3]. Currently, oral rehydration solution is the most important and efficient treatment for cholera[4,5]. However, this therapeutic strategy does not influence bacterial survival or virulence and its effectiveness is limited, particularly in young and elderly patients[6]. In addition, *V. cholerae* isolates resistant to multiple antibiotics are becoming more prevalent[7]. Thus, novel drugs to treat cholera are urgently needed. While phage therapy has potential as an alternative strategy for treatment and prevention of cholera in animal models[8,9], the development of antimicrobial therapy against *V. cholerae* has also recently focused on virulence inhibitors[4].

To cause disease, *V. cholerae* needs to successfully colonize the surface of epithelial cells in the small intestine[10]. The major virulence factors of *V. cholerae* are the toxin co-regulated pilus (TCP), which facilitates the attachment of bacteria to the intestinal epithelium, and cholera toxin (CTX), which enters epithelial cells and causes massive

[1]National Key Laboratory of Intelligent Tracking and Forecasting for Infectious Diseases, TEDA Institute of Biological Sciences and Biotechnology, Nankai University, Tianjin, People's Republic of China. [2]Guangzhou Municipal and Guangdong Provincial Key Laboratory of Molecular Target & Clinical Pharmacology, the NMPA and State Key Laboratory of Respiratory Disease, School of Pharmaceutical Sciences and the Fifth Affiliated Hospital, Guangzhou Medical University, Guangzhou, People's Republic of China. [3]Key Laboratory of Molecular Microbiology and Technology, Nankai University, Ministry of Education, Tianjin, People's Republic of China. [4]Nankai International Advanced Research Institute, Shenzhen, People's Republic of China. [5]These authors contributed equally: Yutao Liu, Jialin Wu, Ruiying Liu. ✉e-mail: guoshengtang@gzhmu.edu.cn; liubin1981@nankai.edu.cn

https://doi.org/10.1038/s41564-024-01823-6

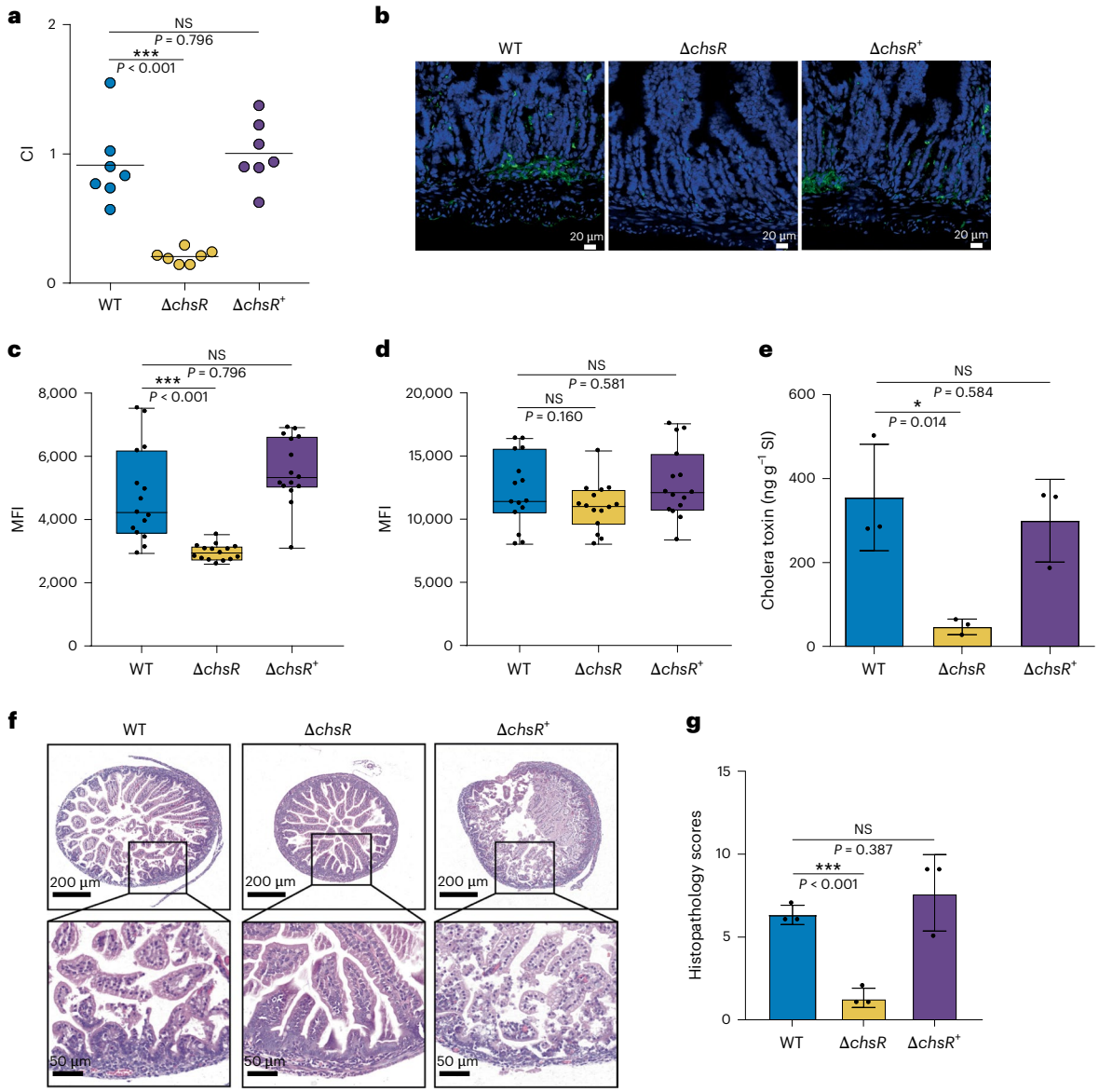

Fig. 1 | The LacI-type regulator ChsR enhances the virulence of *V. cholerae*. **a**, Competition assay comparing the colonization ability of WT, Δ*chsR* and Δ*chsR*$^+$ in the infant mouse intestine ($n = 7$). The CI is defined as the output ratio of mutant strains to WT *lacZ*$^-$ divided by the input ratio of mutant strains to WT *lacZ*$^-$. Each symbol represents the CI in an individual mouse; horizontal bars indicate the median. **b**, The production of cholera toxin by WT, Δ*chsR* or Δ*chsR*$^+$ in the small intestine of mice at 24 h postinfection. The nuclei of mouse intestines were labelled with DAPI (blue), and cholera toxin was labelled with anti-beta subunit cholera toxin antibody (green). **c**,**d**, Mean fluorescence intensity (MFI) analysis of cholera toxin (**c**) and intestinal cells (**d**) in each field. Three visual fields from each mouse were analysed, and five mice were examined. The boxes represent the 25th to 75th percentiles. The whiskers represent minimum and maximum data points. The horizontal bars indicate the median. **e**, Cholera toxin production in the small intestine (SI) of WT, Δ*chsR* or Δ*chsR*$^+$-infected mice was determined by ELISAs ($n = 3$). **f**,**g**, Representation (**f**) and histological score (**g**) of WT, Δ*chsR* and Δ*chsR*$^+$ in the infant mouse intestine 24 h postinfection ($n = 3$). Significance was determined by a two-sided Mann–Whitney *U* test (**a**) or a two-tailed unpaired Student's t-test (**c**,**d**,**e**,**g**) and indicated as the *P* value. $^*P < 0.05$; $^{***}P < 0.001$. Data are presented as mean ± s.d. (**e**,**g**).

secretion of electrolytes and water into the lumen[10,11]. CTX and TCP synthesis is coordinated by a unique regulatory system, including several transcriptional regulators, such as ToxT and TcpP[12]. The expression of *tcpP* is under the control of several regulators: Fur, AphA, AphB and OhrR directly activate *tcpP* expression by binding to its promoter, whereas HapR directly represses *tcpP* expression by binding to its promoter[13–15].

The genome of pandemic *V. cholerae* strains also encodes 11 genes annotated as potential LacI-type regulators, which are widely found across bacteria and often regulate the expression of carbohydrate and nutrient utilization genes in accordance with substrate availability[16,17]. Four of these LacI-type regulators have been functionally characterized in *V. cholerae*, and several have roles potentially involved in virulence or colonization[17–20]. FruI is reported to regulate virulence by influencing intracellular cAMP levels in *V. cholerae*[17], while CytR regulates the expression of genes related to flagellar motility, adhesion and virulence[21]. It is likely that more LacI-type regulators are involved in the regulation of virulence in *V. cholerae*. ChsR is a LacI-type regulator that represses the expression of *chsABC*, which encodes a carbohydrate phosphotransferase system (PTS) for dimers of *N*-glucosamine $(GlcN)_2$ (ref. 18). This substrate is a degradation product of chitin and chitosan, which is an important source of carbon and nitrogen for *V. cholerae*[22] when outside mammalian hosts and in its natural aquatic environment[23].

Here we show that ChsR contributes to the virulence of *V. cholerae* by directly increasing the expression of *tcpP*, which further promotes the production of CTX and TCP. Chitosan oligosaccharide (COS) is an oligomer of GlcN ($(GlcN)_n$), which is produced through the deacetylation and hydrolysis of chitin and chitosan[24]. COS has been recognized as a generally recognized as safe material by the US FDA and is frequently used as a food supplement[25]. We showed that administration of COS effectively suppresses the virulence of *V. cholerae* in vivo by specifically disrupting the *chsR*-mediated pathway. Sodium alginate (SA) microspheres represent a pH-sensitive material that prevents drug degradation by gastric acid and facilitates targeted release within the intestinal tract, suggesting potential for SA microspheres as drug carriers in the treatment of intestinal diseases[26]. In this study, we designed FDA-approved SA microspheres as carriers, using the gas-shearing method for the targeted delivery of COS to the small intestine, thereby enhancing therapeutic efficacy.

Results

ChsR activity increases *V. cholerae* virulence

Comparative genomics analysis revealed that *chsABC* and *chsR* show identical distribution patterns in pandemic and non-pandemic *V. cholerae* strains: they are present in all pandemic strains but only in some non-pandemic strains (Supplementary Dataset 1). It indicates that the acquisition of these genes may confer selective advantages to pandemic strains. To investigate whether *chsR* is also associated with the virulence of *V. cholerae*, in addition to its role in regulating chitosan utilization, we tested whether *chsR* contributes to the colonization ability of bacteria in the small intestine of infant mice. We constructed the deletion mutant Δ*chsR* and the corresponding complemented strain Δ*chsR*$^+$ in the seventh-pandemic strain El2382 (Δ*chsR*$^+$ was generated by introducing a plasmid containing *chsR* with its native promoter into Δ*chsR*). The competitive infection assays in infant mice showed that Δ*chsR* exhibited a significantly defective intestinal colonization ability compared with the wild type (WT) in the small intestine (Fig. 1a), while Δ*chsR*$^+$ competed evenly with WT in the small intestine (Fig. 1a).

Next, we assessed the production of CTX by *V. cholerae* in the small intestine of infant mice. The ileum of mice infected by WT, Δ*chsR* or Δ*chsR*$^+$ and the ileal contents were fixed. Paraffin cross-sections were probed using an antibody against CTX and analysed by immunofluorescence microscopy. In addition, CTX levels in the small intestines of mice infected with WT, Δ*chsR* or Δ*chsR*$^+$ were also measured via enzyme-linked immunosorbent assays (ELISAs). The results showed that the amount of CTX produced by WT or Δ*chsR*$^+$ in the small intestine of mice was significantly higher than that in Δ*chsR*-infected mice (Fig. 1b–e). This indicates that deletion of *chsR* inhibited the production of CTX.

We further investigated the histological damage caused by *V. cholerae* in the small intestine of infant mice and showed that the histopathology scores in WT-infected mice were much higher than those in Δ*chsR*-infected mice (Fig. 1f,g), indicating that the severity of disease caused by Δ*chsR* infection in mice was decreased compared with that of disease caused by WT infection. Collectively, these data indicate that *chsR* contributes to bacterial intestinal colonization and CTX production, leading to enhanced disease intensity in hosts.

ChsR induces virulence gene expression

We first investigated whether the influence of ChsR on the pathogenicity of *V. cholerae* is related to its regulation of the expression of *chsABC*. By analysing the growth of Δ*chsB* or Δ*chsR* in M9 minimal medium supplemented with 0.5% $(GlcN)_2$, we confirmed that ChsB and ChsR are involved in the bacterial uptake of $(GlcN)_2$ (Fig. 2a). The competitive infection assays showed that Δ*chsB* competed similarly to WT in the small intestine of mice (Fig. 2b). Furthermore, we showed that deletion of *chsB* did not influence the expression of virulence genes in vivo and in vitro (Extended Data Fig. 1a,b). This indicates that ChsR does not influence the virulence of *V. cholerae* by regulating the expression of the PTS transporter for $(GlcN)_2$.

RNA sequencing (RNA-seq) revealed that 675 genes were significantly differentially expressed between Δ*chsR* and WT in the small intestine of infant mice (Supplementary Dataset 2). In addition to *chsABC*, which showed increased expression in Δ*chsR*, we observed a decrease in the expression of several known virulence genes in Δ*chsR*, including *tcpP*, *toxT* and *ctxA*, which are involved in the regulation and synthesis of CTX and TCP. The quantitative reverse transcription (qRT)-PCR assays confirmed the decreased expression of these virulence genes in Δ*chsR* compared with WT in vitro and in vivo (Fig. 2c,d). Consistent with this, western blotting assays showed that the production of CTX was significantly decreased in Δ*chsR* compared with that in WT (Fig. 2e,f). These results suggest that *chsR* enhances the expression of virulence factors, which promotes the pathogenicity of *V. cholerae* in vivo.

ChsR directly activates *tcpP* expression

Forty-nine potential binding sites of ChsR on the genome of *V. cholerae* were detected via chromatin immunoprecipitation with sequencing (ChIP-seq) analysis (Supplementary Dataset 3), and these included a site in the promoter region of *tcpP*, which is one of the major virulence regulators in *V. cholerae*[14] (Fig. 3a). As expected, a potential binding site for ChsR was also found in the promoter region of *chsB*. ChIP with quantitative PCR (ChIP-qPCR) assays showed that the *tcpP* and *chsB* promoters both showed significant enrichment of ChsR via binding compared with the control DNA (Fig. 3b), indicating that ChsR directly regulates *tcpP* and *chsB* expression. Furthermore, competitive electrophoretic mobility shift assays (EMSAs) showed that ChsR specifically binds to fluorescein amidite (FAM)-labelled P_{tcpP} or P_{chsB} in a specific manner. Moreover, the addition of unlabelled P_{tcpP} or P_{chsB} effectively competed for ChsR binding to the labelled P_{tcpP} or P_{chsB} (Fig. 3c–e). These results indicate that ChsR specifically binds to the promoter regions of *tcpP* and *chsB*. LacI-type regulators always bind to DNA as dimers[27]. Domain structure predictions revealed a potential dimerization domain in ChsR (Extended Data Fig. 2a), and a cross-linking experiment confirmed that ChsR can form dimers (Extended Data Fig. 2b). Using a dye-based DNase I footprinting assay, we revealed a specific ChsR-bound sequence containing a 34-base-pair motif (5-ATGCAATTAAGTTCTCATTATCAACTGCAGAATT-3) in the promoter region of *tcpP* (Fig. 3f), which was located −108 bp to −74 bp from the proximal transcriptional start site. We also performed competitive EMSAs using a $P_{tcpP\text{-mutant}}$ DNA fragment (without the 34 bp binding site) under the same conditions. The results showed that deletion of the 34 bp binding site completely abolished the binding of ChsR to P_{tcpP} (Fig. 3g). Furthermore, competitive EMSAs were conducted to investigate the binding of ChsR to labelled P_{tcpP} and unlabelled $P_{tcpP\text{-mutant}}$. The results showed that the unlabelled $P_{tcpP\text{-mutant}}$ did not result in a reduction of migrating bands, suggesting that ChsR cannot bind to $P_{tcpP\text{-mutant}}$ (Fig. 3h). These data indicate that ChsR directly regulates the expression of *tcpP* by binding to its promoter region.

We next investigated whether ChsR regulates virulence gene expression in *V. cholerae* via TcpP and constructed the Δ*tcpP* mutant and Δ*tcpP*Δ*chsR* double mutant. As expected, qRT-PCR assays showed that the expression of virulence genes, including *toxT*, *tcpA* and *ctxA*, was significantly reduced in Δ*tcpP* (Fig. 3i). However, deletion of *chsR* had no effect on virulence gene expression and bacterial intestinal colonization ability in a Δ*tcpP* background (Fig. 3i,j), indicating that the regulatory role of ChsR on virulence gene expression is mediated by TcpP. Collectively, these data suggest that ChsR is able to enhance the expression of *tcpP* by directly binding to its promoter region, which results in the increased expression of downstream virulence genes.

AphA, AphB, OhrR and Fur directly activate *tcpP* expression by binding to its promoter[13–15]. To investigate whether these factors influence ChsR's regulation on *tcpP* expression, we constructed Δ*aphB*, Δ*aphA*, Δ*ohrR* and Δ*fur* mutants. As expected, the expression of *tcpP*

https://doi.org/10.1038/s41564-024-01823-6

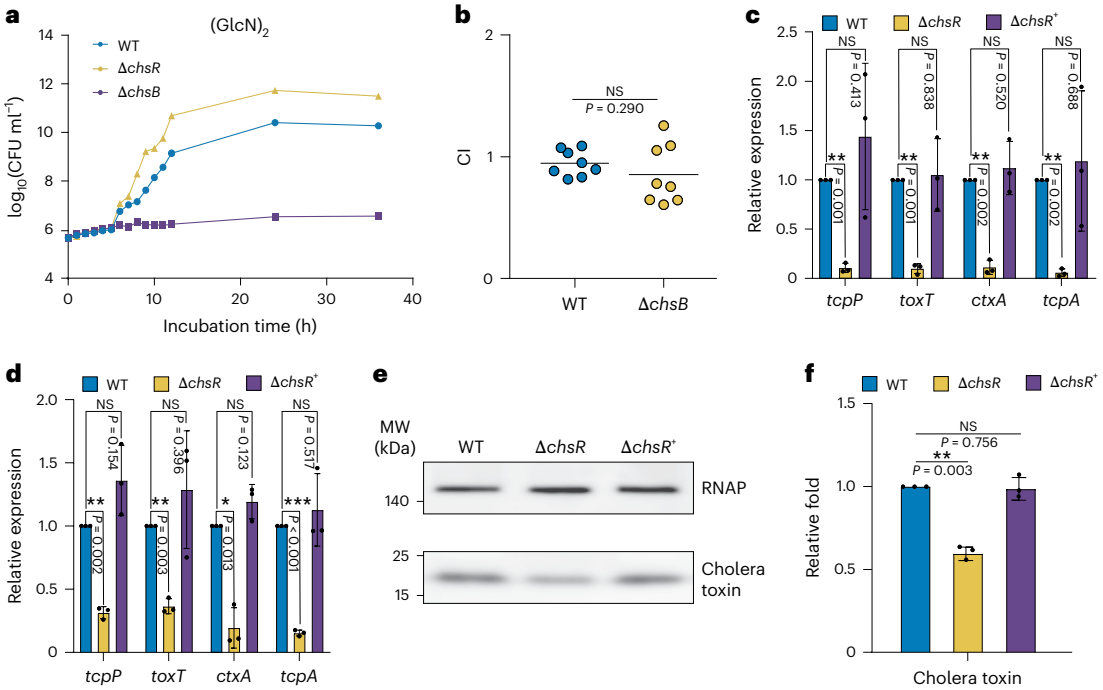

Fig. 2 | ChsR enhances the pathogenicity of *V. cholerae* by regulating the expression of virulence genes but not the PTS for $(GlcN)_2$. **a**, Growth curves of WT, Δ*chsR* and Δ*chsB* in M9 medium containing 0.5% $(GlcN)_2$ as the only carbon source ($n = 3$). **b**, Competition assay comparing the colonization abilities of WT and Δ*chsB* in the infant mouse intestine ($n = 8$). The CI is defined as the output ratio of mutant strains to WT *lacZ*$^-$ divided by the input ratio of mutant strains to WT *lacZ*$^-$. Each symbol represents the CI in an individual mouse; the horizontal bars indicate the median. **c**,**d**, qRT-PCR expression of virulence genes (*tcpP*, *toxT*, *ctxA* and *tcpA*) in WT, Δ*chsR* and Δ*chsR*$^+$ in AKI medium (**c**) or mouse small intestine (**d**) ($n = 3$). **e**,**f**, Representative western blotting image (**e**) and quantitative analysis (**f**) of cholera toxin produced by WT, Δ*chsR* and Δ*chsR*$^+$ in AKI medium. RNAP was used as a loading control ($n = 3$). Significance was determined by a two-sided Mann–Whitney *U* test (**b**) or two-tailed unpaired Student's *t*-test (**c**,**d**,**f**) and indicated as the *P* value. $^*P < 0.05$; $^{**}P < 0.01$; $^{***}P < 0.001$. Data are presented as mean ± s.d. (**a**,**c**,**d**,**f**).

was reduced in all these mutants. We then overexpressed *chsR* in these mutants. qRT-PCR assays showed that overexpression of *chsR* in these mutants restored *tcpP* expression to levels close to those found in the WT (Extended Data Fig. 2c–f). We also found that the deletion of *chsR* in the Δ*aphB*, Δ*aphA*, Δ*ohrR* or Δ*fur* background further decreased the expression of *tcpP* (Extended Data Fig. 2c–f). These data indicate that the regulation of *tcpP* expression by ChsR is not influenced by AphA, AphB, OhrR or Fur.

Low O_2 induces ChsR-mediated virulence via Fnr

qRT-PCR assays showed that the expression of *chsR* in *V. cholerae* showed a significant increase in the small intestine of mice compared with that in Luria–Bertani (LB) medium in vitro (Extended Data Fig. 3a), indicating that *chsR* expression was upregulated in vivo. DNA pull-down assays showed that two regulator proteins (Fnr and Fur) may bind to the promoter region of *chsR* (Supplementary Dataset 4). However, competitive EMSAs showed that only Fnr specifically bound to the promoter region of *chsR*, whereas Fur did not (Extended Data Fig. 3b–e).

Fnr is a global transcription regulator controlling the expression of many genes in response to oxygen starvation[28]. The DNA-binding activity of Fnr under anaerobic conditions is associated with its ability to dimerize, which is regulated by the presence of O_2-labile [4Fe-4S] clusters. Conversely, under aerobic conditions, the [4Fe-4S] clusters are destroyed, and Fnr is converted to an inactive monomeric species, which cannot bind to specific DNA targets[29,30]. qRT-PCR assays showed that the expression of *chsR* in Δ*fnr* was significantly reduced compared with that in WT under in vitro anaerobic conditions, whereas deletion of *fnr* had no effect on *chsR* expression under aerobic conditions (Extended Data Fig. 3f,g). Furthermore, deletion of *fnr* also led to decreased expression of *chsR* in the small intestine of mice in an anaerobic environment (Extended Data Fig. 3h). Consistent with this, *chsR* expression in WT under anaerobic conditions was higher than that under aerobic conditions, and *chsR* expression in Δ*fnr* showed no significant difference between anaerobic and aerobic conditions (Extended Data Fig. 3i). These data indicate that anaerobic conditions, such as the environment in the small intestine, can enhance the expression of *chsR* through the regulator Fnr.

As expected, the expression of *tcpP* was reduced in Δ*fnr* under anaerobic conditions (Extended Data Fig. 3j). Given that Fnr is a global transcription regulator, it is possible that Fnr can influence *tcp* expression independent of ChsR. However, the deletion of *fnr* in the Δ*chsR* background did not result in a further decrease in *tcpP* expression (Extended Data Fig. 3k). Furthermore, the overexpression of *chsR* in Δ*fnr* restored the *tcpP* expression levels to the WT levels (Extended Data Fig. 3j). These data indicate that the influence of Fnr on *tcpP* expression is mediated by ChsR.

In addition, several regulators, including AphB, OhrR and ArcA, are capable of sensing low O_2 levels in *V. cholerae*[14,17]. In addition, OhrA is a thiol-dependent, peroxidase-like protein that responds to redox changes in the gastrointestinal tract[31]. We showed that the deletion of *aphB*, *ohrR*, *arcA* or *ohrA* had no effect on *chsR* expression under anaerobic conditions in vitro or in the small intestine of mice (Extended Data Fig. 3l). It indicates that these factors are not involved in the pathway through which low O_2 levels induce *chsR* expression.

Collectively, these data indicate that the *chsR*-mediated virulence regulatory pathway is activated by Fnr in response to the low O_2 signal in the small intestine of the host.

$(GlcN)_2$ and GlcN inhibit ChsR-mediated virulence gene induction

It is likely that inhibiting the interaction between ChsR and the promoter region of *tcpP* may result in decreased expression of downstream

https://doi.org/10.1038/s41564-024-01823-6

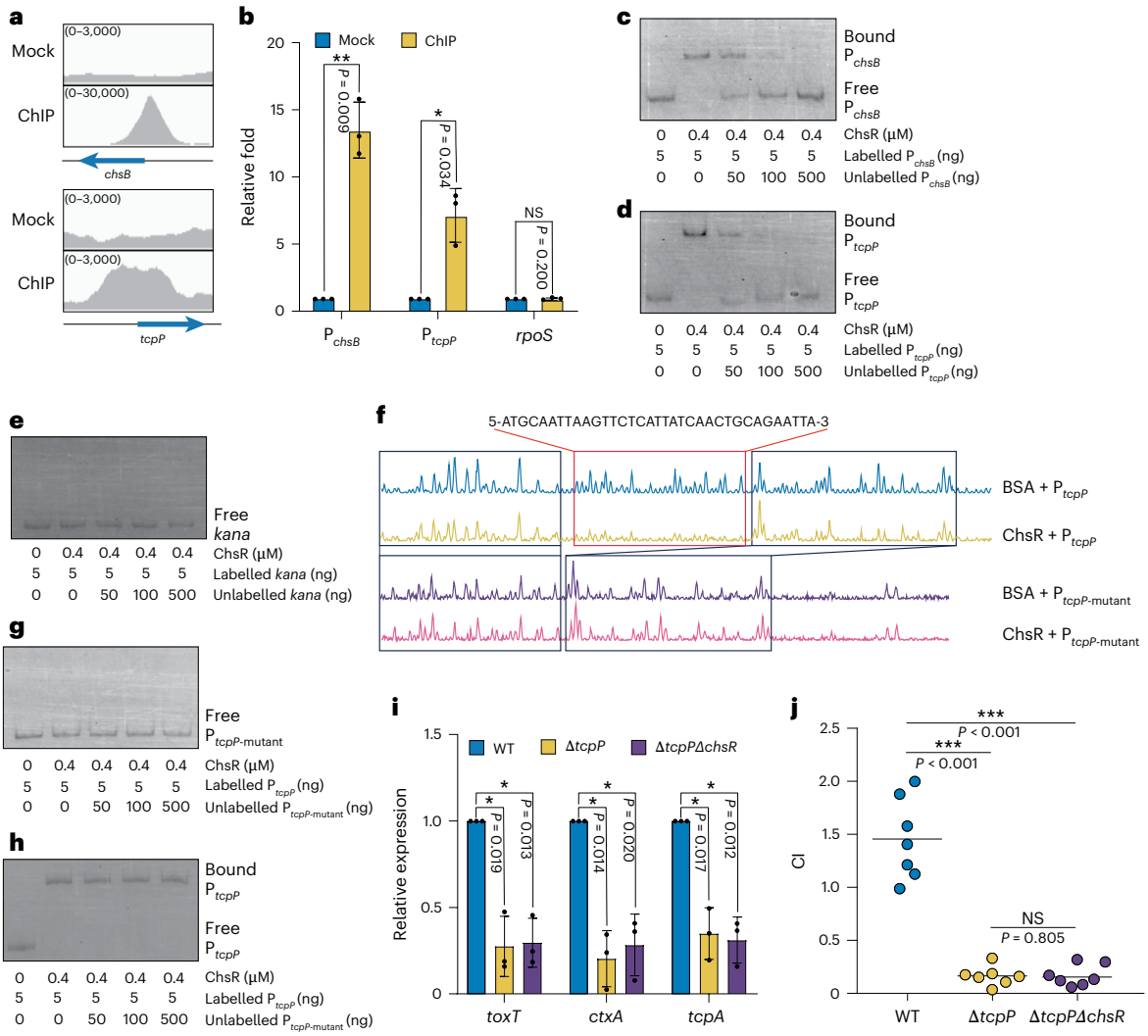

Fig. 3 | ChsR directly activates the expression of *tcpP*, leading to increased expression of downstream virulence genes. a, Original sequence peaks of the ChsR-binding regions in P_{chsB} and P_{tcpP} according to ChIP-seq analyses. **b**, Fold enrichment of P_{chsB}, P_{tcpP} and the coding region of *rpoS* in ChsR-ChIP samples, as measured by qRT-PCR. *rpoS* served as a negative control ($n = 3$). **c**–**e**, Competitive EMSAs of ChsR binding to FAM-labelled and unlabelled P_{chsB} (**c**), P_{tcpP} (**d**) and *kana* (**e**, negative control, an irrelevant DNA fragment that was amplified from the kanamycin-resistant gene of the pKD4 plasmid). **f**, ChsR binds to a motif in P_{tcpP} (this motif is deleted in the $P_{tcpP\text{-mutant}}$). The protected region shows a significantly reduced peak intensity and is highlighted by the red box. BSA was used as a negative control. **g**, Competitive EMSAs of ChsR binding to FAM-labelled and unlabelled $P_{tcpP\text{-mutant}}$. **h**, Competitive EMSAs of ChsR binding to FAM-labelled P_{tcpP} and unlabelled $P_{tcpP\text{-mutant}}$. **i**, qRT-PCR analysis of virulence gene (*tcpP*, *toxT*, *ctxA* and *tcpA*) expression in the WT, Δ*tcpP* and Δ*chsR*Δ*tcpP* strains in the mouse small intestine ($n = 3$). **j**, Competition assay comparing the colonization abilities of WT, Δ*tcpP* and Δ*chsR*Δ*tcpP* strains in the infant mouse intestine ($n = 7$). The CI is defined as the output ratio of mutant strains to the WT *lacZ*$^-$ strain divided by the input ratio of mutant strains to the WT *lacZ*$^-$ strain. Each symbol represents the CI for an individual mouse; the horizontal bars indicate the median. Significance was determined by a two-sided Mann–Whitney *U* test (**j**) or two-tailed unpaired Student's t-test (**b**,**i**) and indicated as the *P* value. $^*P < 0.05$; $^{**}P < 0.01$; $^{***}P < 0.001$. Data are presented as mean ± s.d. (**b**,**i**). The results are representative of three biological replicate experiments (**c**–**e**,**g**,**h**).

virulence genes. The repression effect of LacI-type regulators on carbohydrate metabolic and transport genes is always released when the corresponding carbohydrate is present and binds to the carbohydrate-binding domain of the regulator. As ChsR regulates the expression of *chsABC*, which encodes a PTS transporter for $(GlcN)_2$, which can be degraded to GlcN within the cytoplasm of *V. cholerae*[32], we hypothesized that $(GlcN)_2$ and GlcN may inhibit the interaction between ChsR and target DNA.

EMSAs showed that the binding of ChsR to the promoters of *tcpP* and *chsB* was inhibited by $(GlcN)_2$ and GlcN (Fig. 4a,b). By contrast, the DNA-binding ability of ChsR was not affected by GlcNAc or glucose (Extended Data Fig. 4a,b). Furthermore, the surface plasmon resonance (SPR) assay showed that $(GlcN)_2$ and GlcN (but not GlcNAc and glucose) were able to interact with purified ChsR protein (Fig. 4c and Extended Data Fig. 4c). Then, the full-length structure of ChsR was predicted by using the AlphaFold Protein Structure Database (Q9KSH0_VIBCH), followed by docking with $(GlcN)_2$ and GlcN (Extended Data Fig. 4d). The docking results showed a stable interaction between $(GlcN)_2$ and GlcN bound to ChsR through hydrogen bonds, van der Waals interactions and pi–pi interactions (Fig. 4d). Furthermore, the docking results revealed the indispensability of Arg194 in facilitating the binding of ChsR to both $(GlcN)_2$ and GlcN (Fig. 4d).

To identify the crucial amino acids responsible for the binding of $(GlcN)_2$ and GlcN to ChsR, R194Q ChsR and R194A ChsR were generated. EMSAs revealed that the DNA-binding ability of R194Q ChsR or R194A ChsR was not affected by $(GlcN)_2$ or GlcN (Extended Data Fig. 4e–h), which is different from the results found for wild-type ChsR. Both R194Q ChsR and R194A ChsR can form stable dimers (Extended Data Fig. 2b).

https://doi.org/10.1038/s41564-024-01823-6

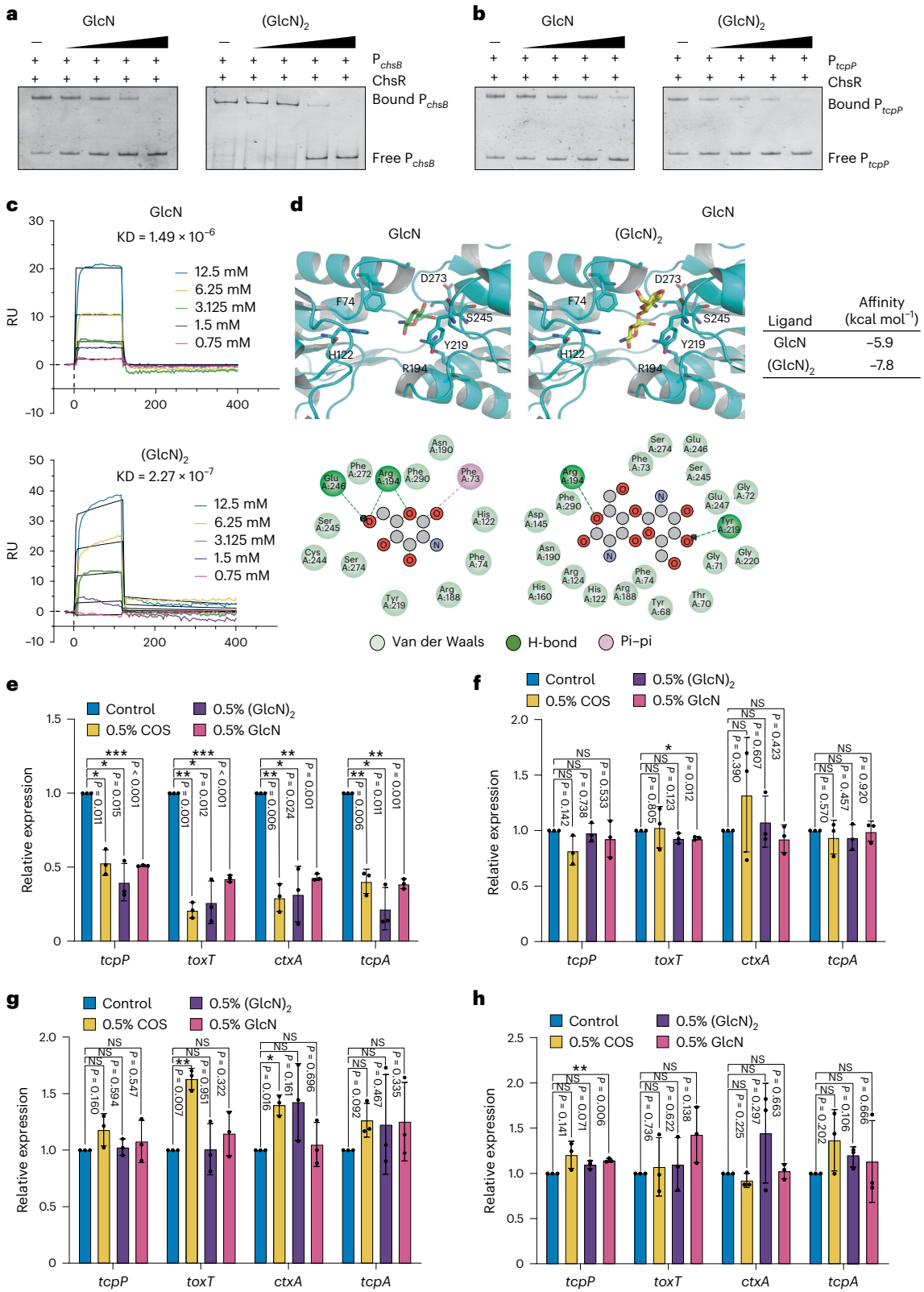

Fig. 4 | $(GlcN)_2$ and GlcN decrease virulence gene expression in *V. cholerae* by inhibiting the interaction between ChsR and the promoter region of *tcpP*. **a**,**b**, The influence of GlcN and $(GlcN)_2$ on the binding of purified ChsR protein to the promoter region of *chsB* (**a**) and *tcpP* (**b**). EMSAs of 0.2 μM purified ChsR protein complexed with 30 ng of the DNA fragment in the presence of different concentrations of putative substrates (0–10 mM) were conducted. **c**, Biacore SPR kinetic analyses of GlcN and $(GlcN)_2$ binding to ChsR. Sensorgram and saturation curve of the titration of different substrates on ChsR immobilized on a CM5 chip. **d**, Two- and three-dimensional docking poses showing the interactions of GlcN and $(GlcN)_2$ with ChsR (AlphaFold Protein Structure Database: Q9KSH0_VIBCH). Interactions are colour coded: bright green represents conventional hydrogen bonds, light green represents van der Waals interactions and pink represents pi–pi interactions. **e**–**h**, qRT-PCR expression level of virulence genes of WT (**e**) or Δ*chsR* (**f**), Δ*chsR*$^+$(R194Q) (**g**) or Δ*chsR*$^+$(R194A) (**h**) in M9 medium containing 0.5% GlcN, $(GlcN)_2$ or COS as the only carbon source ($n = 3$). Significance was determined by a two-tailed unpaired Student's *t*-test (**e**–**h**) and indicated as the *P* value. $^*P < 0.05$; $^{**}P < 0.01$; $^{***}P < 0.001$. Data are presented as mean ± s.d. (**e**–**h**). Results are representative of three biological replicate experiments (**a**,**b**).

In addition, we introduced a plasmid containing *chsR* with the R194Q or R194A mutation into the Δ*chsR* strain, generating the Δ*chsR*$^+$(R194Q) and Δ*chsR*$^+$(R194A) strains. qRT-PCR assays revealed that *tcpP* expression in the Δ*chsR*$^+$(R194Q) and Δ*chsR*$^+$(R194A) strains did not significantly differ from that in the WT and Δ*chsR*$^+$ strains (Extended Data Fig. 4i). This finding indicates that the R194Q or R194A mutation did not affect the stability or function of ChsR in activating the expression of *tcpP*. Collectively, these data indicate that $(GlcN)_2$ and GlcN can bind to ChsR and inhibit its interaction with the promoters of *tcpP* and *chsB*.

The structure of COS is similar to that of chitosan. By cultivating bacteria in M9 medium supplemented with 0.5% COS, we found that the WT strain, but not the Δ*chsB* strain, can use COS as its sole carbon source (Extended Data Fig. 4j). This finding indicates that *V. cholerae* can use COS in the same manner as it does with chitosan. Furthermore, we showed that incubation with $(GlcN)_2$, GlcN or COS significantly decreased the expression of virulence genes in the WT strain in vitro (Fig. 4e). However, treatment of the Δ*chsR*, Δ*chsR*$^+$(R194Q) or Δ*chsR*$^+$(R194A) strains with $(GlcN)_2$, GlcN or COS had no influence on virulence gene expression in the bacteria (Fig. 4f–h). Collectively, these data indicate that $(GlcN)_2$, GlcN and COS can reduce virulence gene expression in *V. cholerae* by inhibiting the function of ChsR.

COS inhibits *V. cholerae* virulence via ChsR in mice

Next, we investigated whether administration of COS could reduce the virulence of *V. cholerae* in vivo in an adult mouse model in which the mice were treated with a cocktail of four antibiotics (Fig. 5a). We showed that in this model, WT can colonize the small intestine of mice, and the deletion of *tcpA*, *toxT*, *tcpP* or *chsR* significantly reduced the bacterial intestinal colonization ability compared with that of the WT in vivo (Extended Data Fig. 5a). These findings indicate that this model can be used to analyse the virulence of *V. cholerae*. qRT-PCR assays showed that virulence gene expression in WT (but not Δ*chsR*, Δ*chsR*$^+$(R194Q) or Δ*chsR*$^+$(R194A)) in adult mice fed COS at a concentration of 0.5% was significantly decreased compared with that in mice that did not receive COS (Fig. 5b,c and Extended Data Fig. 5b,c). We found that colonization by WT in the small intestine of mice that were administered 0.5–2% COS at the time of bacterial oral challenge was significantly lower than that in mice that did not receive COS (the inhibitory effect of COS on the colonization of *V. cholerae* peaked at a COS concentration ≥0.5%) (Fig. 5d). By contrast, COS administration had no effect on the colonization by Δ*chsR*, Δ*chsR*$^+$(R194Q) or Δ*chsR*$^+$(R194A) in the small intestine of mice, which is different from what was observed for WT and Δ*chsR*$^+$ (Extended Data Fig. 5d,e). In addition, we also showed that the histological damage caused by WT (but not Δ*chsR*) in mice that were administered COS at the time of challenge was decreased compared with that in mice that did not receive COS (Fig. 5e,f and Extended Data Fig. 5f,g). Collectively, these data indicate that by inhibiting the function of ChsR, the presence of COS in the small intestine resulted in the reduced virulence of *V. cholerae* in vivo, leading to decreased disease intensity in the hosts.

Furthermore, we investigated the potential of COS as a preventive agent against *V. cholerae* infection. We showed that colonization by WT in the small intestine of adult mice, which were administered COS at concentrations >1% for three consecutive days before the bacterial challenge, was significantly decreased compared with that in mice that did not receive COS (Fig. 5g). These data indicate that administration of COS is probably an effective strategy to prevent *V. cholerae* infection. The fact that a relatively high concentration (>1%) of COS was required for preventing *V. cholerae* infection in animal experiments (as described above, feeding mice ≥0.5% COS at the time of bacterial oral challenge can inhibit bacterial virulence) may be attributed to the use of COS by the gut microbiota.

COS NPs@microspheres inhibit cholera in mice

To improve the efficacy of COS in the treatment and prevention of cholera, we innovatively designed SA microspheres loaded with COS nanoparticles to target the intestinal tract. A schematic diagram of COS nanoparticles encapsulated in SA microspheres (COS NPs@microsphere, CNM) preparation is shown in Fig. 6a, and Fig. 6b–e shows the morphology of CNMs under bright-field microscopy, scanning electron microscopy (SEM) and fluorescence microscopy. COS nanoparticles with green fluorescence were uniformly distributed in the SA microspheres with red fluorescence. Furthermore, the gas-shearing method could be easily used to fabricate microparticles with different sizes and very high monodispersity (Extended Data Fig. 6a–f). Herein, considering the feasibility of oral administration, microspheres of 300–500 μm were selected for the following experiments (Fig. 6f).

We further investigated the stability and release of the CNMs in the gastrointestinal tract. As shown in Fig. 6g–j, the ratio of fluorescence intensity did not change significantly in phosphate-buffered saline (PBS) and simulated gastric fluid (SGF) but markedly increased in simulated intestinal fluid (SIF) after 3 h and had almost 100% after 21 h, indicating that SA protected COS from degradation in SGF and prolonged its retention in SIF.

We observed the distribution of CNMs with an in vivo imaging system (IVIS) after oral administration. CNMs could be detected in the small intestine 6 h after administration and were completely eliminated in the ileum and colon at 24 h (Fig. 6k,l), indicating that the microspheres effectively protected COS from being damaged by the stomach and could accumulate in the intestine.

We further investigated the potential of CNMs as a preventive measure against *V. cholerae* infection (Fig. 5a). Using the adult mouse model, we found that the colonization by WT (but not Δ*chsR*$^+$(R194Q) or Δ*chsR*$^+$(R194A)) in the small intestine of mice that were administered CNMs at a concentration of 0.5% for three consecutive days before bacterial challenge was significantly decreased compared with that in mice that received COS (Fig. 6m,n). This indicates that, compared with COS, CNMs provide more favourable outcomes in the treatment and prevention of cholera.

Several studies have shown that COS has antimicrobial activity[33]. To show that the administration of COS or CNMs reduces the virulence of *V. cholerae* in vivo by blocking the ChsR-mediated virulence pathway but not by influencing the viability of *V. cholerae*, we compared the number of *V. cholerae* cells within the intestinal lumen of mice treated with PBS, 0.5% COS or 0.5% CNMs (it should be noted that the colonization ability of *V. cholerae* was assessed by measuring the efficiency of in vivo bacterial attachment to the intestinal epithelium, as described in Methods). The results showed no significant difference among the groups, indicating that neither COS nor CNMs had an effect on *V. cholerae* survival (Fig. 6o). Furthermore, growth curve analysis revealed that supplementation with COS at a concentration of 0.5% or CNMs at a concentration of 2% had no inhibitory effect on the growth of *V. cholera* (Extended Data Fig. 6g,h). These data suggest that the concentrations of COS and CNMs administered to the mice in our experiments did not impact the survival of *V. cholerae*. These data also indicate that the therapeutic effect of COS or CNMs on *V. cholerae* infection is due to their influence on the function of ChsR rather than their antimicrobial effects.

Discussion

ChsR is previously known to repress the expression of *chsABC* when chitosan is not available for *V. cholerae*[18]. This enables *V. cholerae* to avoid unnecessary energy waste in expressing the PTS when chitosan is unavailable, which may benefit bacterial survival in aquatic environments. Until now, only a limited number of LacI-type regulators have been identified to play a role in regulating bacterial virulence, such as FruI and CytR in *V. cholerae*[17,21], Cra in enterohaemorrhagic *Escherichia coli* and PurR in *Staphylococcus aureus*[34,35]. In this study, we showed that *chsR* expression is induced in the small intestine of the host by the low O_2 signal, which promotes the production of CTX and TCP in this infection site, leading to enhanced bacterial pathogenicity in the host.

https://doi.org/10.1038/s41564-024-01823-6

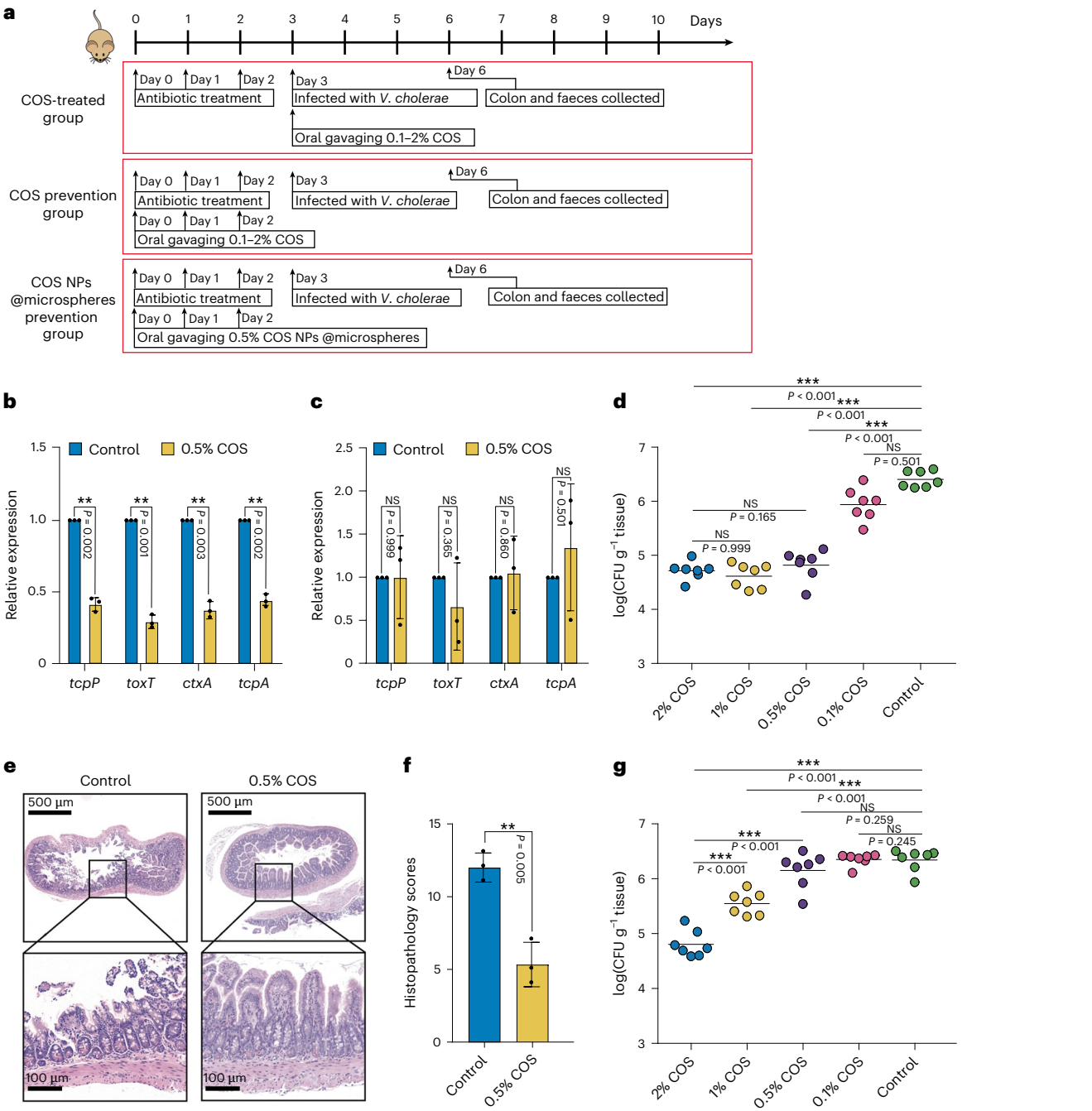

Fig. 5 | COS shows potential as a promising drug candidate for both therapeutic and preventive interventions against cholera. a, Schematic of *V. cholera* colonization in different infection models. **b**,**c**, qRT-PCR expression levels of virulence genes (*tcpP*, *toxT*, *ctxA* and *tcpA*) of WT (**b**) or Δ*chsR* (**c**) in the small intestine of adult mice administered 0.5% COS at 24 h postinfection ($n = 3$). **d**, Evaluation of the colonization ability of WT in the small intestine of adult mice administered 0.1–2% COS at the time of bacterial oral challenge at 3 days postinfection ($n = 7$). **e**,**f**, Representation (**e**) and histological score (**f**) of WT in the small intestine of adult mice administered 0.5% COS at 3 days postinfection ($n = 3$). **g**, Evaluation of the colonizing ability of WT in the small intestine of adult mice administered 0.1–2% COS on days 1, 2 and 3 before bacterial challenge at 3 days postinfection ($n = 7$). Significance was determined by a two-sided Mann–Whitney *U* test (**d**,**g**) or two-tailed unpaired Student's *t*-test (**b**,**c**,**f**) and indicated as the *P* value. $^*P < 0.05$; $^{**}P < 0.01$; $^{***}P < 0.001$. Data are presented as mean ± s.d. (**b**,**c**,**f**).

These facts suggest that *chsR* contributes to both the in vivo virulence and environmental fitness of *V. cholerae*.

Several strategies, such as recombination-based in vivo expression technology and transposon insertion site sequencing, have previously been used to identify essential genes for the in vivo fitness of *V. cholerae*. The recombination-based in vivo expression technology results revealed that the insertion mutant *chsR* showed a severe colonization defect in infant rabbits[36]. However, the recombination-based in vivo expression technology analysis did not identify *chsR* as an in vivo-induced gene during infection in infant mice[37,38]. The discrepancy in these results may be attributed to variations in the animal model and the timing of sample collection.

Although previous studies showed that ChsR repressed the expression of *chsABC* (ref. 18), it remains unclear whether ChsR directly represses the expression of these genes or acts via other regulators. We showed that ChsR binds to the promoter of *chsB* directly (Fig. 3c). This

https://doi.org/10.1038/s41564-024-01823-6

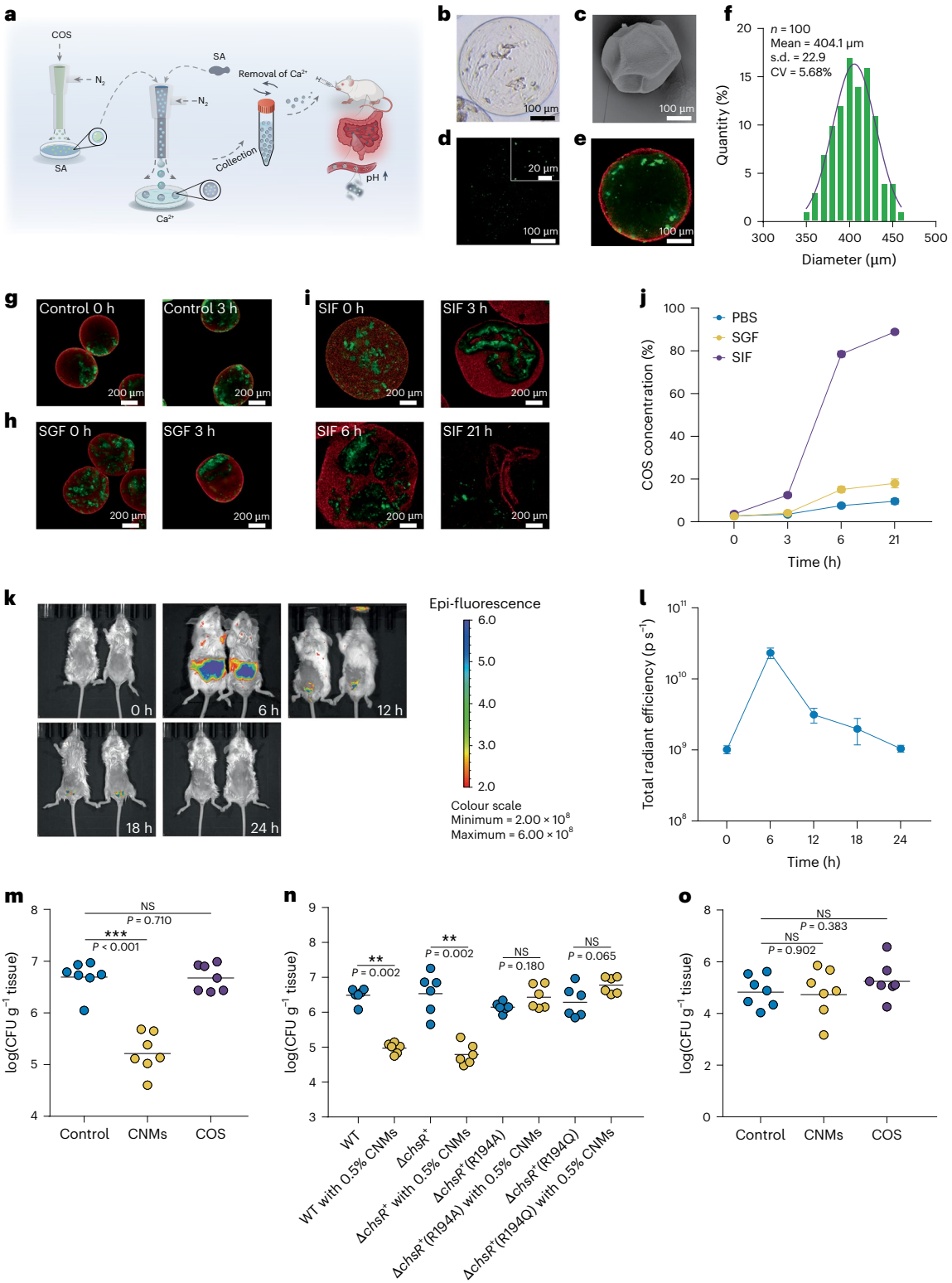

Fig. 6 | CNMs are an effective therapeutic drug for *V. cholerae* infection. **a**, Schematic illustration of the fabrication process for CNMs. **b**, Bright-field images of CNMs. **c**, SEM image of CNMs. **d**,**e**, Fluorescence images of COS nanoparticles (green) (**d**) and CNMs (SA, red) (**e**). **f**, The diameter distribution of CNMs. CV, coefficient of variation. **g**–**i**, Fluorescence microscopy images of CNMs in PBS (**g**), SGF (**h**) and SIF (**i**) over time. **j**, The release of COS in three solutions detected by ultraviolet spectrophotometer. **k**, IVIS imaging of two representative mice at different time points following oral administration of CNMs. **l**, Total fluorescence radiant efficiency in animals injected with CNMs ($n = 6$). **m**, Evaluation of the colonization ability of WT in the small intestine of adult mice after administration of 0.5% CNMs or COS for three consecutive days before bacterial challenge ($n = 7$). **n**, Evaluation of the colonization ability of WT, Δ*chsR*$^+$, Δ*chsR*$^+$(R194A) and Δ*chsR*$^+$(R194Q) in the small intestine of adult mice with or without administration of 0.5% CNMs for three consecutive days before bacterial challenge ($n = 6$). **o**, Evaluation of the luminal survival capability of WT in the small intestine of adult mice after administration of 0.5% CNMs or COS for three consecutive days before bacterial challenge ($n = 7$). Significance was determined by a two-sided Mann–Whitney *U* test (**m**–**o**) and indicated as the *P* value. $^*P < 0.05$; $^{**}P < 0.01$; $^{***}P < 0.001$. Data are presented as mean ± s.d. (**j**,**l**). Results are representative of three biological replicate experiments (**b**–**e**).

indicates that when COS is used to reduce the virulence gene expression of *V. cholerae* by inhibiting the interaction between ChsR and the *tcpP* promoter region in vivo, the repression of *chsABC* expression by ChsR is also released. This may benefit the growth of *V. cholerae* by promoting the uptake of $(GlcN)_2$. However, as carbon sources that can be used by *V. cholerae*, such as glucose and fructose, are relatively abundant in the small intestine[17], it is likely that the slight increase in available carbon sources due to the administration of low-concentration COS will not influence the growth of *V. cholerae* in vivo. Indeed, we obtained experimental evidence that the survival of *V. cholerae* in the intestinal lumen of mice administered COS showed no significant changes compared with that in normal mice (Fig. 6o). Therefore, we suggest that administration of COS reduces the virulence of *V. cholerae* without influencing the growth of bacteria in the small intestine of hosts.

Currently, cholera remains an important human health problem worldwide. Recently, for the development of therapeutic strategies against cholera, many studies have focused on the identification of inhibitors targeting the virulence factors of *V. cholerae*. In this study, we showed that administration of COS could specifically repress the ChsR-mediated virulence regulatory pathway of *V. cholerae* (Extended Data Fig. 7) and, thus, results in a significant decrease in bacterial intestinal colonization and disease severity in animal models. This treatment targets the virulence of *V. cholerae* but not bacterial growth, and thus, selection for resistant bacteria should be greatly reduced compared with that under antibiotic treatment. Compared with most inhibitors for *V. cholerae* virulence that would be expensive to produce, COS is a commercially available biopolymer that has been shown to hold essential value in the pharmaceutical, biomedical and nutraceutical fields[33,39]. It has several advantages in application, such as its widespread use, low cost, convenient administration, and ease of storage and transportation. Therefore, COS has the potential to be used as a supplemental cholera therapy in conjunction with oral rehydration and as a preventive drug for *V. cholerae* infection (Extended Data Fig. 7). Furthermore, we took on the challenge of designing CNMs by gas shearing. Compared with the direct oral administration of COS, CNMs can prevent the degradation of COS in the gastric environment and achieve sustained release in the intestine, which could effectively improve COS bioavailability.

Methods

Ethics statement

All animal experiments were performed according to the standards set forth by the Guide for the Care and Use of Laboratory Animals. All animal studies were conducted according to protocols approved by the Institutional Animal Care Committee of Nankai University (Tianjin, China) and performed under protocol number IACUC 2016030502.

Bacterial strains, plasmids and growth conditions

The bacterial strains and plasmids used in this study are listed in Supplementary Datasets 5 and 6. *V. cholerae* O1 El Tor strain El2382 was provided by Shanghai Municipal Centers for Disease Control and Prevention. *E. coli* BL21 (DE3) was used for recombinant protein expression. The *E. coli* S17/λpir strain was used for conjugation. The bacterial strains were grown in LB broth, M9 medium or AKI medium (1.5% Bacto Peptone, 0.4% yeast extract, 0.5% NaCl and 0.3% $NaHCO_3$)[40]. For aerobic conditions, bacteria were grown at 37 °C with shaking at 180 rpm (ref. 20). For anaerobic conditions, bacteria were grown at 37 °C in an anaerobic incubator (YQX-II), and oxygen-free nitrogen was used as the carrier gas[41]. Antibiotics were used at the following concentrations: polymyxin B, 40 μg ml^{-1}; ampicillin, 50 μg ml^{-1}; chloramphenicol, 25 μg ml^{-1}; and kanamycin, 50 μg ml^{-1}.

Mutant construction and complementation

All primers used in this study are listed in Supplementary Dataset 7. Construction of the mutants was performed using the suicide vector pRE112 (ref. 42). The pBAD33 vector was used for complementation by cloning genes with native promoters. *chsR* and its promoter region were cloned in frame with pBAD33 along with the C-terminal 3×FLAG. *chsR*, R194Q *chsR*, R194A *chsR*, *fnr* and *fur* were cloned into pET28a for protein purification. For overexpression, *chsR* was cloned into the pTrc99A vector. R194Q *chsR* and R194A *chsR* were synthesized by Azenta Life Sciences.

Growth curve

To determine bacterial growth curves in M9 medium with 0.5% $(GlcN)_2$, COS or CNMs, overnight cultures were washed with M9 medium three times and diluted to 10^6 ml^{-1} in a flask containing 20 ml of M9 medium with $(GlcN)_2$, COS or CNMs and incubated at 37 °C with shaking at 180 rpm. A 100 μl aliquot was removed from the flask and diluted on LB agar plates. The growth rate was determined by counting cells hourly. Three experiments were performed independently.

RNA isolation and qRT-PCR

To detect gene expression in vivo, samples were collected from the small intestine of mice. To analyse virulence gene expression in vitro, samples were collected from AKI medium under aerobic conditions or from M9 medium with 0.5% GlcN, 0.5% $(GlcN)_2$ or 0.5% COS. To analyse the expression of *chsR* in vitro, samples were incubated in LB medium to reach stationary phase. To analyse the expression of *chsR* in an anaerobic environment, samples were collected and incubated under aerobic or anaerobic conditions. We isolated total RNA using TRIzol reagent (15596026) and measured its concentration using a NanoDrop 2000 spectrophotometer (Thermo Fisher Scientific). In three independent experiments, cDNA was synthesized using the PrimeScript RT Reagent Kit with gDNA Eraser (Takara). To conduct qRT-PCR analysis, we used an Applied Biosystems ABI 7500 with SYBR green fluorescence dye. The *rrsA* gene was used as a reference control to normalize sample data, and relative expression levels were calculated as fold change values using the $2^{-\Delta\Delta CT}$ method. Each experiment was performed in triplicate.

RNA-seq

The small intestines of three mice were collected after colonization by the WT and Δ*chsR* strains. For library preparation, 1 μg of total RNA with an RNA integrity number (RIN) value > 8.0 was isolated using TRIzol Reagent (Invitrogen). Libraries were constructed and analysed using Majorbio. The Benjamini and Hochberg method was used to adjust *P* values to control the false discovery rate when identifying genes with a differential expression (|fold change| > 2 and $P = 0.05$). All sequence data have been deposited in the National Center for Biotechnology Information Sequence Read Archive (NCBI SRA) database under accession code PRJNA900711.

Western blotting

The *V. cholerae* strains were grown overnight and diluted 1:100 in fresh AKI medium. After being grown anaerobically for 4 h and reaching an optical density of 0.2, the cultures were shaken for 2–2.5 h to reach an optical density of 1.0. After collecting, washing and resuspending the bacteria in PBS at 4 °C, we sonicated the samples for 15 cycles at 95% power for 30 s. A centrifuge was used to remove the debris from the cells after centrifuging at 12,000 × *g* for 10 min at 4 °C. The supernatants were quantified using the bovine serum albumin (BSA) method. A 4–12% gel was used to separate equal amounts of total protein. Vocation membranes (Bio-Rad) were electroblotted onto PVDF membranes (Bio-Rad) after the protein was separated. Blots for RNA polymerase (RNAP) and cholera toxin were incubated with anti-RNA polymerase beta (ab191598) and anti-beta subunit cholera toxin antibody (ab123129) at a dilution of 1:2,000. The blots were further incubated with goat anti-rabbit IgG secondary antibody (1:5,000 dilution; EF0002, Shandong Sparkjade Biotechnology) tagged with horseradish peroxidase. Detection was carried out using a Sparkjade ECL Plus (ED0016, Shandong Sparkjade Biotechnology) detection system. Images were acquired using an Amersham Imager 600 system (General Electric).

EMSA

The 6×His-tagged Fnr, Fur, native ChsR, R194Q ChsR and R194A ChsR proteins were expressed and purified in *E. coli* BL21 (DE3). For competition assays, DNA fragments were amplified with or without 6-FAM-labelled primers and purified using the SPARKeasy Gel DNA Extraction Kit (AE0101, Shandong Sparkjade Biotechnology). The purified DNA probe (5 ng) was incubated at 25 °C for 30 min with 0.4 μM 6×His-tagged protein in 20 μl solutions prepared in binding buffer (5 mM HEPES (pH 7.9), 1 mM dithiothreitol, 0.1 mM ethylenediaminetetraacetic acid (EDTA), 40 mM KCl and 5% glycerol), and various concentrations of unlabelled DNA fragments (0 to 500 ng) were added. A native polyacrylamide gel was electrophoretically separated at 4 °C and 90 V cm^{-1}, and the labelled fragments were visualized with an Amersham Imager 600 (GE Healthcare). For ligand screening studies, purified native ChsR, R194Q ChsR and R194A ChsR were incubated in binding buffer containing 0–10 mM GlcN, $(GlcN)_2$, GlcNAc or glucose at 25 °C for 10 min before incubation with unlabelled DNA fragments. The protein bands on the gel were visualized by ultraviolet transillumination after 10 min of staining with 0.1% GelRed.

ChIP and qPCR

Bacteria were grown at 37 °C to mid-exponential phase, and expression was induced with L-arabinose. After centrifugation, 1% formaldehyde was added and the sample was incubated for 25 min at approximately 25 °C. The sample was then mixed with 0.5 M glycine. A further 5 min of incubation terminated the cross-linking reaction. Cross-linked bacteria were collected after 5 min of incubation and were washed three times with ice-cold PBS. Re-suspended cross-linked bacteria were incubated at 37 °C for 30 min in lysis buffer (10 mM Tris (pH 7.5), 1 mM EDTA, 100 mM NaCl, 1 mM protease inhibitor cocktail, 1 mg ml^{-1} lysozyme, 0.1 mg ml^{-1} RNase A). Then, immunoprecipitation buffer (100 mM Tris–HCl (pH 7.5), 200 mM NaCl, 1 mM EDTA, 2% v/v Triton X-100, 1 mM phenylmethane sulfonyl fluoride) was incubated, and the lysates were further sonicated to generate DNA fragments of approximately 300 bp. After centrifugation at 12,000 × *g* for 10 min, supernatants were incubated with Monoclonal ANTI-FLAG M2 antibody (number F1804; Sigma-Aldrich) and protein A magnetic beads (Invitrogen; number 10002D). DNA samples were subsequently purified using a PCR purification kit (number 28104; Qiagen). A next-generation sequencing library was prepared and sequenced by Novogene after ChsR-ChIP and mock–ChIP DNA were collected. All sequence data have been deposited in the NCBI SRA database under accession code PRJNA963002.

To determine ChsR-binding peak enrichment, ChIP–qPCR was carried out using an Applied Biosystems ABI 7500. The *rpoS* gene (non-specific enrichment) was used as a reference. The relative enrichment of candidate targets was calculated as fold enrichment using the formula $2^{-\Delta\Delta CT}$. Experiments were independently performed three times.

Dye primer-based DNase I footprinting assay

DNase I footprinting assays were modified from published procedures[43]. Approximately 300 bp fragments of the P_{tcpP} or $P_{tcpP\text{-mutant}}$ were generated by PCR with 6-FAM primers. ChsR protein or BSA (negative control) protein was added to 40 ng of 6-FAM-labelled *tcpP* promoter in binding buffer (10 mM Tris–HCl (pH 7.5), 0.2 mM dithiothreitol, 5 mM $MgCl_2$, 10 mM KCl and 10% glycerol) at concentrations ranging from 0.8 μM. Then, 0.05 U DNase I (Sigma; AMPD1) was added to the 20 μl solution for 10 min at 37 °C. Heat at 85 °C for 10 min in the presence of 250 mM EDTA stopped the reaction. PCR fragments were purified using a QIAquick PCR Purification Kit (Qiagen; number 28104) and eluted in 15 μl of distilled water. The samples were analysed using MAP Biotech. The results were analysed using a peak scanner (Applied Biosystems).

DNA affinity pull-down assay

DNA pull-down assays were performed as previously described[44]. Briefly, the biotin-labelled DNA fragment containing the promoter region of *chsR* was amplified from strain E12382. The biotinylated bait DNA was bound to streptavidin-coated Dynabeads (catalogue number 11205D; Invitrogen), followed by incubation with crude extracts obtained from E12382 WT cells. An elution buffer containing 500 mM NaCl was used to release bound proteins after extensive washing with the nonspecific competitor poly (dI-dC). Proteins were separated using SDS–PAGE and stained with Coomassie brilliant blue. After tryptic digestion, proteins were excised from the gel and analysed using matrix-assisted laser desorption ionization–time-of-flight tandem mass spectrometry. Sequence and peptide fingerprint data were analysed using the NCBI database. The proteomics data were submitted to the iProX (integrated proteome resources) (subproject ID: IPX0008142000).

Surface plasmon resonance screening

Analyses of ligand binding and binding kinetics were performed at 25 °C on a Biacore X100 (BR110073). All experiments were carried out with PBS as the running buffer with a constant flow rate of 10 μl min^{-1} at 25 °C. ChsR was diluted with 10 mmol l^{-1} sodium acetate buffer (pH 5.0) to a final concentration of 10 μM. A 1-ethyl-3-(3-dimethylaminopropyl) carbodiimide and N-hydroxysuccinimide (EDC–NHS) cross-linking reaction was used to immobilize ChsR on the surface of a CM5 Sensor Chip. At a flow rate of 10 μl min^{-1}, small molecules were diluted with running buffer from 0.75 mM to 12.5 mM and injected into the reference channel and ChsR channel at the target immobilization level of 3,600 response units. Both coupling and dissociation times were 120 s. Biacore X100 evaluation software was used to fit the affinity curves using a steady-state affinity model (1:1). The equilibrium dissociation constant (KD) was calculated.

Molecular docking

The Protein Data Bank (PDB) file of ChsR was generated using AlphaFold Protein Structure Database (https://www.alphafold.com/search/text/Q9KSH0_VIBCH). The AutoDock Vina program was used to predict the site of binding of ligands to ChsR (ref. 45). First, the protein and ligand PDBQT files for docking were generated using AutoDockTools 1.5.6 (ref. 46). During PDBQT file preparation, polar hydrogen atoms and Kollman united atom partial charges were added to the protein atoms. Meanwhile, Gasteiger charges were assigned to the ligand molecules. ChsR was programmed to remain rigid while the ligand was flexible. The size of the box was set to 24 Å. The centre of the box was in the catalytic activity centre. Subsequently, the docking conformation with the lowest binding energy was selected to analyse the binding mode. Discovery Studio visualizer was used to analyse noncovalent interactions between ligands and ChsR. Visualization and analysis of model features were performed using Open-Source PyMOL.

Infant mouse colonization assay

The infant mouse intestinal colonization assay was used to evaluate the pathogenic capacity of *V. cholerae* strains. Both sexes of 5-day-old CD-1 mice were purchased from Beijing Vital River Laboratory Animal Technology and placed in incubators at 30 °C and a relative humidity of 50 ± 5%, and housed under specific-pathogen-free conditions with a 12 h light–dark cycle. An in vivo competition assay for intestinal colonization was performed as previously described with minor modifications[47]. Briefly, both the *V. cholerae lacZ*$^+$ (wild-type) and *lacZ*$^-$ (Δ*lacZ*) strains were cultured overnight at 37 °C with shaking in LB medium. Approximately 10^5 *lacZ*$^+$ cells were mixed with an equal number of *lacZ*$^-$ cells, and the mixtures were intragastrically administered to groups of eight anaesthetized mice. To determine the recovery of bacteria and the output ratios, the small intestine was removed from each mouse, weighed, homogenized and plated on LB agar plates containing 5-bromo-4-chloro-3-indoyl-D-galactopyranoside (X-gal). The competitive index (CI) was determined as the output ratio of *lacZ*$^+$ to *lacZ*$^-$ cells divided by the input ratio of *lacZ*$^+$ to *lacZ*$^-$ cells.

Adult mouse colonization (attachment) assay

The adult mouse intestinal colonization assay was used to evaluate the prophylactic and therapeutic efficacy of COS and CNMs. An adult mouse colonization assay was performed as previously described[48]. Six-week-old female specific-pathogen-free BALB/c mice were purchased from Beijing Vital River Laboratory Animal Technology and placed in incubators at 30 °C and a relative humidity of 50 ± 5% and housed under specific-pathogen-free conditions with a 12 h light–dark cycle. The mice were orally administered a cocktail of four antibiotics, namely, ampicillin, neomycin, metronidazole and vancomycin (Sigma-Aldrich), via oral gavage for 3 days to deplete the gut microbiota (5 mg of each antibiotic per mouse per day). When necessary, varying concentrations of COS or CNMs were orally administered. Food was removed from cages to empty the stomach 20–24 h before inoculation. The mice were first fed 50 µl of 8.5% (wt/vol) sodium bicarbonate intragastrically, followed immediately by 50 µl of the bacterial suspension in PBS containing 10^9 colony-forming unit (CFU) by oral gavage. After inoculation, the mice were provided with ad libitum access to aseptic water and food devoid of streptomycin. Infected mice were anaesthetized and euthanized by cervical dislocation 3 days after infection. The small intestines were excised from the infected animals and subsequently washed three times with PBS. The intestinal tissues and/or contents were weighed and homogenized in 0.5 ml of PBS, after which the homogenates were diluted and plated on LB agar. The in vivo attachment efficiency was determined by counting the number of CFU per gram of intestine.

Cholera toxin detection

The secretion of cholera toxin was detected via the GM1-ELISA method[49]. The microwell plates were initially coated with GM1 ganglioside (MedChemExpress, 37758-47-7) and incubated overnight to ensure adequate coating. For the establishment of a standard curve, purified cholera toxin subunit B (Absin, 131096-89-4) was used. BSA served as a negative control. Small intestines infected with each *V. cholerae* strain were extracted under sterile conditions and homogenized to prepare tissue homogenates. Aliquots of these homogenates were analysed via the ELISA protocol. Following the ELISA procedure, the optical density (OD) at 450 nm of the samples was measured using a Spark 10M multimode microplate reader (Tecan).

Immunohistochemistry on cryosections

The small intestines of infected infant and adult mice were collected for analysis. The collected samples were fixed in 4% paraformaldehyde, washed with PBS, incubated overnight in 30% sucrose at 4 °C, embedded in Tissue-Tek OCT (Sakura, 4583) and stored at −80 °C. Sections 8 µm thick were cut with a CM 1850 UV cryomicrotome (Leica) and placed on a glass slide.

Immunostaining of frozen tissue sections was performed as described previously[50]. Briefly, slides were defrosted at room temperature (RT) for 5 min in a wet chamber. For fixation, the slides were immersed in methanol (70%) for 90 s. After fixation, the slides were washed (3 × 5 min) with PBS (0.1 M). To reduce nonspecific antibody binding, tissues were kept in PBS containing 5% BSA (Solarbio, SW3015) for 1 h at RT and then incubated with anti-beta subunit cholera toxin antibody (ab62429) diluted in PBS containing 5% BSA at 4 °C overnight. The tissue sections were washed with PBS five times and then incubated with fluorophore-conjugated secondary antibody, goat anti-mouse FITC (ab6785), diluted in PBS containing 5% BSA at RT for 1 h. After washing with PBS five times, the cell nuclei were stained with 5% DAPI (Bioss, C02-04002) at RT for 5 min. Coverslips were then mounted on the slides with ProLong anti-fade reagent (Sangon Biotech, E675011). The tissue sections were visualized using a Zeiss LSM800 confocal microscope (Carl Zeiss).

Histological analysis

The small intestines of infected adult and infant mice were collected for analysis. The small intestines were fixed in 10% neutral buffered formalin overnight and embedded in paraffin. Paraffin-embedded sections were deparaffinized and stained with haematoxylin–eosin. Then, the stained sections were blindly scored for inflammation severity. The histologic score was calculated based on the intensity of mononuclear and polymorphonuclear infiltrates in the neutrophil infiltration (0–3), changes in the architecture of the mucosa (0–3), villus height (0–3), goblet cell depletion (0–3), integrity of the epithelium (0–3) and attached bacteria (0–3). For each parameter, the changes were graded according to the following scale: 0, absent; 1, mild; 2, moderate; and 3, intense[51].

Preparation of COS nanoparticles and CNMs

Both COS nanoparticles and CNMs were prepared through a cytocompatible oil-free gas-shearing method. Solutions and devices were sterilized before use. First, the COS aqueous solution (50%) was introduced into the coaxial nozzle device, and then the COS solution was broken down into nanoscale droplets under the shear force (7.0 l min^{-1}) of nitrogen, which was collected and solidified in a low concentration of SA (0.2%). Afterwards, the concentration of SA obtained from the previous step was increased from 0.2% to 1% and injected into the coaxial nozzle device to prepare uniform droplets under a flow of 2.0 l min^{-1}, and then the SA droplet was cross-linked with the collecting bath ($CaCl_2$, 2%) to form CNMs. Finally, these microspheres were collected and washed three times to remove the residual calcium ions on the surface before use.

Characterization of CNMs

COS and SA were labelled with green (Q-W012580, Ruixibio) and red fluorescent nanoparticles (Rigor Biotechnology), respectively. The optical and fluorescence images of COS nanoparticles and CNMs were obtained by fluorescence microscopy (MSHOT MF53-N) and laser scanning confocal microscopy (ELYPA P.1, Zeiss). The diameter of the CNMs was measured using ImageJ software. The freeze-dried microspheres were observed by SEM (Phenom Pure, Thermo) for surface appearance and internal structure.

Degradation test of CNMs

The prepared CNMs were immersed in three different solutions at once, including PBS, SGF and SIF (pH = 7). All three groups were incubated at 37 °C. Finally, we evaluated the integrity of microspheres using CLSM at a specified time of 1–21 h.

Analysis of the release of COS from CNMs

The CNMs were immersed in PBS, SGF or SIF (pH 7) for 0–21 h. The absorbance of the supernatant from each group was evaluated after filtering using an ultraviolet–visible spectrophotometer at 202 nm. Each experiment was performed in triplicate.

Bioluminescence imaging

Bioluminescence imaging was performed using an IVIS Spectrum (PerkinElmer) imaging scanner coupled to Living Image Software (PerkinElmer). Briefly, at different time points, 100 µl of 0.5% fluorescent CNMs (the SA of the CNMs was mixed with green fluorescent nanoparticles) was administered orally to each mouse. Before scanning, the abdominal cavity of the mice was shaved to allow accurate collection of fluorescent signals. Bioluminescence images were acquired after execution via cervical dislocation and quantified using imaging software.

Glutaraldehyde cross-link assay

A glutaraldehyde cross-link assay was performed based on previously published procedures with modifications[46]. Briefly, the 6×His-tagged native ChsR, R194Q ChsR and R194A ChsR proteins were expressed and purified in *E. coli* BL21 (DE3). Glutaraldehyde was then added to 100 µg of purified native ChsR, R194Q ChsR or R194A ChsR protein, resulting in a final concentration of 0.001% in 20 µl of solution. After 20 min of

incubation, the reactions were terminated by adding 5 µl of 5×SDS–PAGE protein loading buffer. Equal amounts of total protein (25 µg) were separated by SDS–PAGE using an 8% gel. Images were acquired with an Amersham Imager 600 system (GE Healthcare).

Statistical analyses

No statistical methods were used to pre-determine sample sizes, but our sample sizes are similar to those reported in previous publications[17,52]. Animals were randomly assigned to control and manipulation groups and data collection. Experimenters were unaware of the experimental conditions of the mice at the time of testing. Other data collection was not randomized, but always done in parallel with controls. There were no exclusions of animals or data points reported.

Data were analysed using *t*-tests, two-way ANOVA or Mann–Whitney *U* tests as indicated in the specific figure legends. Values with $P < 0.05$, 0.01 or 0.001 were considered statistically significant (*), highly significant (**) or extremely significant (***), respectively; NS represents no significance. Data distribution was assumed to be normal, but this was not formally tested. Figures were drawn using GraphPad 7.

Reporting summary

Further information on research design is available in the Nature Portfolio Reporting Summary linked to this article.

Data availability

Relevant data are given within the Article, Supplementary Data files and Source Data files. RNA-seq data have been deposited in the NCBI SRA database under accession code PRJNA900711. ChIP-seq data have been deposited in the NCBI SRA database under accession code PRJNA963002. The proteomics data were submitted to the iProX (integrated proteome resources) (subproject ID: IPX0008142000). Source data are provided with this paper.

Code availability

No custom code was used or developed for the analysis of data presented in this study.

References

1. Hu, D. et al. Origins of the current seventh cholera pandemic. *Proc. Natl Acad. Sci. USA* **113**, E7730–E7739 (2016).
2. Ali, M. et al. The global burden of cholera. *Bull. World Health Organ.* **90**, 209–218A (2012).
3. Conner, J. G., Teschler, J. K., Jones, C. J. & Yildiz, F. H. Staying alive: *Vibrio cholerae*'s cycle of environmental survival, transmission, and dissemination. *Microbiol. Spectr.* **4**, VMBF-0015-2015 (2016).
4. Sousa, F. B. M. et al. A comprehensive review of therapeutic approaches available for the treatment of cholera. *J. Pharm. Pharmacol.* **72**, 1715–1731 (2020).
5. Chowdhury, F., Ross, A. G., Islam, M. T., McMillan, N. A. J. & Qadri, F. Diagnosis, management, and future control of cholera. *Clin. Microbiol. Rev.* **35**, e0021121 (2022).
6. Tradtrantip, L., Ko, E. A. & Verkman, A. S. Antidiarrheal efficacy and cellular mechanisms of a Thai herbal remedy. *PLoS Negl. Trop. Dis.* **8**, e2674 (2014).
7. Kitaoka, M., Miyata, S. T., Unterweger, D. & Pukatzki, S. Antibiotic resistance mechanisms of *Vibrio cholerae*. *J. Med. Microbiol.* **60**, 397–407 (2011).
8. Yen, M., Cairns, L. S. & Camilli, A. A cocktail of three virulent bacteriophages prevents *Vibrio cholerae* infection in animal models. *Nat. Commun.* **8**, 14187 (2017).
9. Bhandare, S. et al. Reviving phage therapy for the treatment of cholera. *J. Infect. Dis.* **219**, 786–794 (2019).
10. Almagro-Moreno, S., Pruss, K. & Taylor, R. K. Intestinal colonization dynamics of *Vibrio cholerae*. *PLoS Pathog.* **11**, e1004787 (2015).
11. Harris, J. B., LaRocque, R. C., Qadri, F., Ryan, E. T. & Calderwood, S. B. Cholera. *Lancet* **379**, 2466–2476 (2012).
12. Silva, A. J. & Benitez, J. A. *Vibrio cholerae* biofilms and cholera pathogenesis. *PLoS Negl. Trop. Dis.* **10**, e0004330 (2016).
13. Gao, H. et al. Direct binding and regulation by Fur and HapR of the intermediate regulator and virulence factor genes within the ToxR virulence regulon in *Vibrio cholerae*. *Front. Microbiol.* **11**, 709 (2020).
14. Liu, Z. et al. Differential thiol-based switches jump-start *Vibrio cholerae* pathogenesis. *Cell Rep.* **14**, 347–354 (2016).
15. Kovacikova, G., Lin, W. & Skorupski, K. *Vibrio cholerae* AphA uses a novel mechanism for virulence gene activation that involves interaction with the LysR-type regulator AphB at the tcpPH promoter. *Mol. Microbiol.* **53**, 129–142 (2004).
16. Heidelberg, J. F. et al. DNA sequence of both chromosomes of the cholera pathogen *Vibrio cholerae*. *Nature* **406**, 477–483 (2000).
17. Liu, Y. et al. A fructose/H^+ symporter controlled by a LacI-type regulator promotes survival of pandemic *Vibrio cholerae* in seawater. *Nat. Commun.* **12**, 4649 (2021).
18. Berg, T., Schild, S. & Reidl, J. Regulation of the chitobiose–phosphotransferase system in *Vibrio cholerae*. *Arch. Microbiol.* **187**, 433–439 (2007).
19. Watve, S. S., Thomas, J. & Hammer, B. K. CytR is a global positive regulator of competence, type VI secretion and chitinases in *Vibrio cholerae*. *PLoS ONE* **10**, e0138834 (2015).
20. Yoon, C.-K., Kang, D., Kim, M.-K. & Seok, Y.-J. *Vibrio cholerae* FruR facilitates binding of RNA polymerase to the *fru* promoter in the presence of fructose 1-phosphate. *Nucleic Acids Res.* **49**, 1397–1410 (2021).
21. Das, S. et al. Multifunctional transcription factor CytR of *Vibrio cholerae* is important for pathogenesis. *Microbiology* **166**, 1136–1148 (2020).
22. Meibom, K. L. et al. The *Vibrio cholerae* chitin utilization program. *Proc. Natl Acad. Sci. USA* **101**, 2524–2529 (2004).
23. Reidl, J. & Klose, K. E. *Vibrio cholerae* and cholera: out of the water and into the host. *FEMS Microbiol. Rev.* **26**, 125–139 (2002).
24. Markov, E. Y., Kulikalova, E. S., Urbanovich, L. Y., Vishnyakov, V. S. & Balakhonov, S. V. Chitin and products of its hydrolysis in *Vibrio cholerae* ecology. *Biochemistry* **80**, 1109–1116 (2015).
25. Liaqat, F. & Eltem, R. Chitooligosaccharides and their biological activities: a comprehensive review. *Carbohydr. Polym.* **184**, 243–259 (2018).
26. Chen, G. L. et al. Chitosan/alginate nanoparticles for the enhanced oral antithrombotic activity of clam heparinoid from the clam *Coelomactra antiquata*. *Mar. Drugs* **20**, 136 (2022).
27. Porcheron, G., Kut, E., Canepa, S., Maurel, M.-C. & Schouler, C. Regulation of fructooligosaccharide metabolism in an extra-intestinal pathogenic *Escherichia coli* strain. *Mol. Microbiol.* **81**, 717–733 (2011).
28. Septer, A. N., Bose, J. L., Dunn, A. K. & Stabb, E. V. FNR-mediated regulation of bioluminescence and anaerobic respiration in the light-organ symbiont *Vibrio fischeri*. *FEMS Microbiol. Lett.* **306**, 72–81 (2010).
29. Isabella, V. M. & Clark, V. L. Deep sequencing-based analysis of the anaerobic stimulon in *Neisseria gonorrhoeae*. *BMC Genomics* **12**, 51 (2011).
30. Crack, J., Green, J. & Thomson, A. J. Mechanism of oxygen sensing by the bacterial transcription factor fumarate–nitrate reduction (FNR). *J. Biol. Chem.* **279**, 9278–9286 (2004).
31. Liu, Z. et al. Thiol-based switch mechanism of virulence regulator AphB modulates oxidative stress response in *Vibrio cholerae*. *Mol. Microbiol.* **102**, 939–949 (2016).
32. Hunt, D. E., Gevers, D., Vahora, N. M. & Polz, M. F. Conservation of the chitin utilization pathway in the Vibrionaceae. *Appl. Environ. Microbiol.* **74**, 44–51 (2008).

33. Muanprasat, C. & Chatsudthipong, V. Chitosan oligosaccharide: biological activities and potential therapeutic applications. *Pharmacol. Ther.* **170**, 80–97 (2017).
34. Njoroge, J. W., Gruber, C. & Sperandio, V. The interacting Cra and KdpE regulators are involved in the expression of multiple virulence factors in enterohemorrhagic *Escherichia coli*. *J. Bacteriol.* **195**, 2499–2508 (2013).
35. Sause, W. E. et al. The purine biosynthesis regulator PurR moonlights as a virulence regulator in *Staphylococcus aureus*. *Proc. Natl Acad. Sci. USA* **116**, 13563–13572 (2019).
36. Fu, Y., Waldor, M. K. & Mekalanos, J. J. Tn-Seq analysis of *Vibrio cholerae* intestinal colonization reveals a role for T6SS-mediated antibacterial activity in the host. *Cell Host Microbe* **14**, 652–663 (2013).
37. Osorio, C. G. et al. Second-generation recombination-based in vivo expression technology for large-scale screening for *Vibrio cholerae* genes induced during infection of the mouse small intestine. *Infect. Immun.* **73**, 972–980 (2005).
38. Schild, S. et al. Genes induced late in infection increase fitness of *Vibrio cholerae* after release into the environment. *Cell Host Microbe* **2**, 264–277 (2007).
39. Naveed, M. et al. Chitosan oligosaccharide (COS): an overview. *Int. J. Biol. Macromol.* **129**, 827–843 (2019).
40. Iwanaga, M. et al. Culture conditions for stimulating cholera toxin production by *Vibrio cholerae* O1 El Tor. *Microbiol. Immunol.* **30**, 1075–1083 (1986).
41. Wagner, A.O. et al. Medium preparation for the cultivation of microorganisms under strictly anaerobic/anoxic conditions. *J. Vis. Exp.* https://doi.org/10.3791/60155 (2019).
42. Xu, T. et al. RNA-seq-based monitoring of gene expression changes of viable but non-culturable state of *Vibrio cholerae* induced by cold seawater. *Environ. Microbiol. Rep.* **10**, 594–604 (2018).
43. Wu, J. et al. MlrA, a MerR family regulator in *Vibrio cholerae*, senses the anaerobic signal in the small intestine of the host to promote bacterial intestinal colonization. *Gut Microbes* **14**, 2143216 (2022).
44. Liu, Y. et al. Magnesium sensing regulates intestinal colonization of enterohemorrhagic *Escherichia coli* O157:H7. *mBio* **11**, e02470-20 (2020).
45. Trott, O. & Olson, A. J. AutoDock Vina: improving the speed and accuracy of docking with a new scoring function, efficient optimization, and multithreading. *J. Comput. Chem.* **31**, 455–461 (2010).
46. Morris, G. M. et al. AutoDock4 and AutoDockTools4: automated docking with selective receptor flexibility. *J. Comput. Chem.* **30**, 2785–2791 (2009).
47. Cheng, A. T., Ottemann, K. M. & Yildiz, F. H. *Vibrio cholerae* response regulator VxrB controls colonization and regulates the type VI secretion system. *PLoS Pathog.* **11**, e1004933 (2015).
48. Toh, Y. S. et al. Role of coaggregation in the pathogenicity and prolonged colonisation of *Vibrio cholerae*. *Med. Microbiol. Immunol.* **208**, 793–809 (2019).
49. You, J. S. et al. Commensal-derived metabolites govern *Vibrio cholerae* pathogenesis in host intestine. *Microbiome* **7**, 132 (2019).
50. Ramadan, T. et al. Basolateral aromatic amino acid transporter TAT1 (Slc16a10) functions as an efflux pathway. *J. Cell. Physiol.* **206**, 771–779 (2006).
51. Liu, B. et al. *Escherichia coli* O157:H7 senses microbiota-produced riboflavin to increase its virulence in the gut. *Proc. Natl Acad. Sci. USA* **119**, e2212436119 (2022).
52. Liu, Y. et al. *Vibrio cholerae* senses human enteric α-defensin 5 through a CarSR two-component system to promote bacterial pathogenicity. *Commun. Biol.* **5**, 559 (2022).

Acknowledgements

This study was supported by the National Key R&D Program of China grant 2022YFC2305302 (to B.L.); the National Natural Science Foundation of China (NSFC) grants 32100144 (to Y.L.), 32070130 (to B.L.), 32201183 (to G.T.) and 82372267 (to B.L.); the Distinguished Young Scholar of Tianjin grant 20JCJQJC00180 (to B.L.); and the Natural Science Foundation of Shenzhen grants JCYJ20220530164604010 (to B.L.), JCYJ20230807151559009 (to B.L.), Guangdong Basic and Applied Basic Research Foundation grant 2024A1515010588 (to B.L.), Key Laboratory Major Project of Tianjin in 2024 (to B.L.) and the Fundamental Research Funds for the Central Universities (to B.L.).

Author contributions

B.L., G.T. and Y.L. designed the research. Y.L., J.W., R.L., F.L., L.X., Q.W., D.L., X.C., H.S, X.L., C.J., D.H. and L.L. performed the experiments. F.L., L.X., Q.W. and R.L. contributed new reagents or analytic tools. Y.L., J.W., L.X., Q.W. and R.L. analysed the data. B.L., G.T., Y.L. and J.W. wrote the paper. All authors gave final approval for the version to be published.

Competing interests

The authors declare no competing interests.

Additional information

Extended data is available for this paper at https://doi.org/10.1038/s41564-024-01823-6.

Supplementary information The online version contains supplementary material available at https://doi.org/10.1038/s41564-024-01823-6.

Correspondence and requests for materials should be addressed to Guosheng Tang or Bin Liu.

Peer review information *Nature Microbiology* thanks Wenguo Cui, Brian Hammer, Matthew Waldor, Julia van Kessel and the other, anonymous, reviewer(s) for their contribution to the peer review of this work. Peer reviewer reports are available.

https://doi.org/10.1038/s41564-024-01823-6

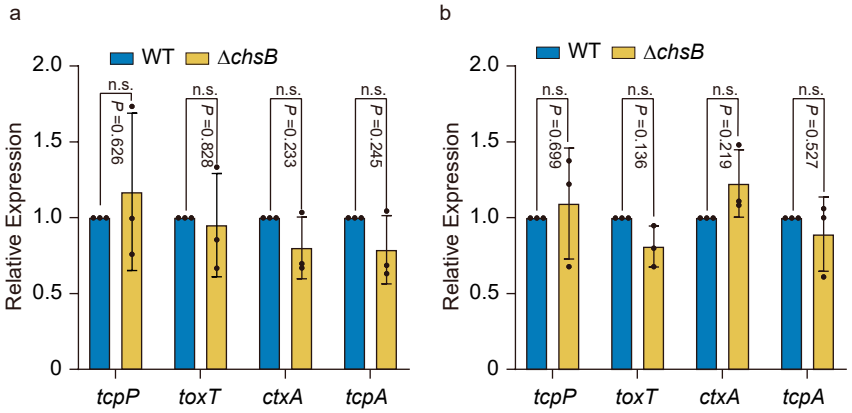

Extended Data Fig. 1 | *chsB* did not influence the expression of virulence genes *in vivo* and *in vitro*. **a**, **b**, qRT–PCR expression levels of virulence genes (*tcpP*, *toxT*, *ctxA* and *tcpA)* in WT and Δ*chsB* in AKI medium (a) and the mouse small intestine (b) (n = 3). Significance was determined by a two-tailed unpaired Student's t test and indicated as the P value. *P < 0.05, **P < 0.01, ***P < 0.001; n.s. no significant difference. Data are presented as mean ± s.d. Source data are included in the Extended Source Data file.

https://doi.org/10.1038/s41564-024-01823-6

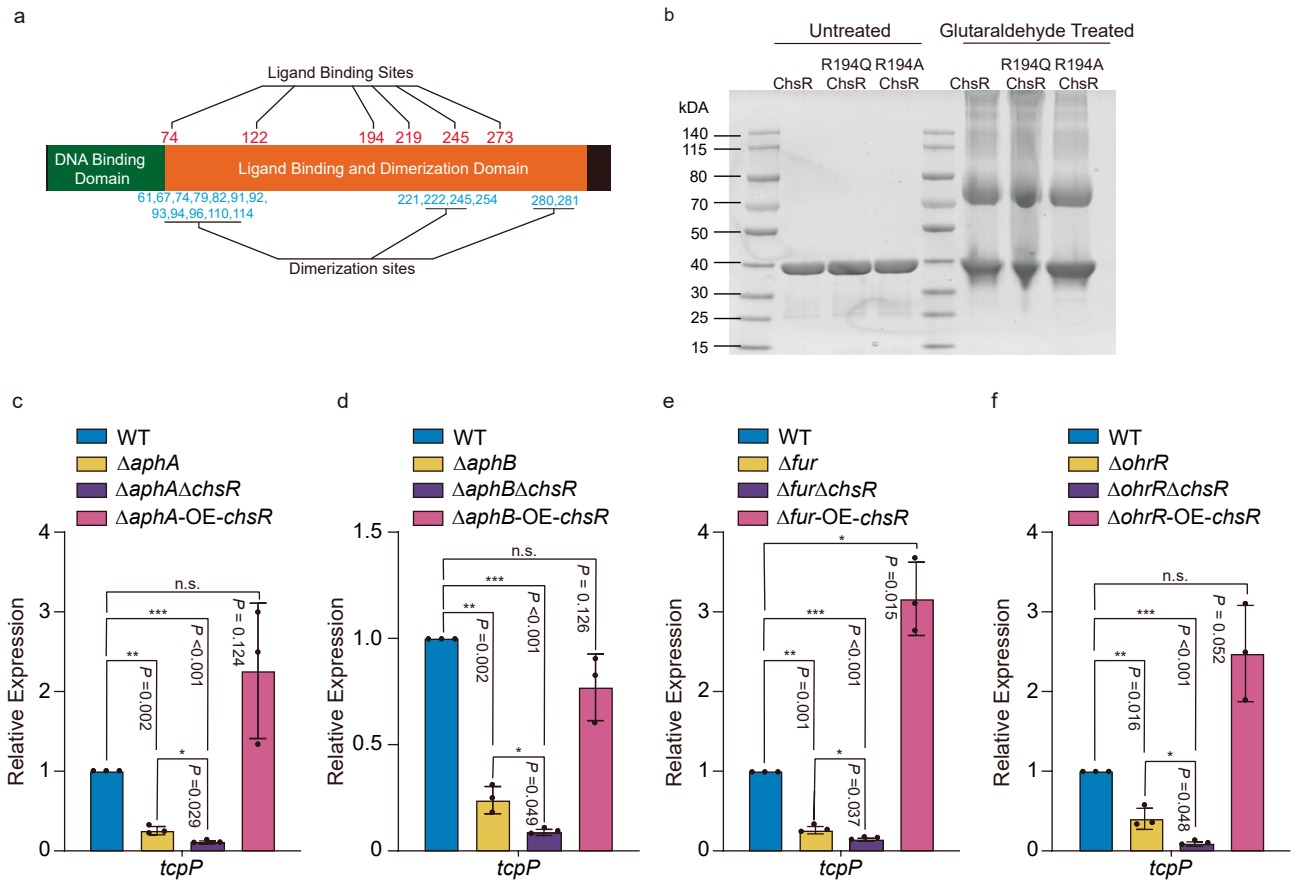

Extended Data Fig. 2 | The regulation of *tcpP* expression by ChsR is not influenced by AphA, AphB, OhrR or Fur. a, Analysis of the conserved domain structure of ChsR. Color coding: black, full-length ChsR; green, DNA-binding domain; orange, ligand-binding domain. The predicted ligand-binding sites are highlighted with red text, and the predicted dimerization sites are highlighted with blue text. **b**, Oligomerization state of ChsR. ChsR was treated with glutaraldehyde and analyzed by SDS–PAGE. Results are representative of three biological replicate experiments. **c**, qRT–PCR expression levels of *tcpP* in the WT, Δ*aphA*, Δ*aphA*Δ*chsR*, and Δ*aphA*-OE-*chsR* (Δ*aphA* with a plasmid containing *chsR* with the trc promoter) strains in AKI medium under anaerobic conditions. **d**, qRT–PCR expression levels of *tcpP* in the WT, Δ*aphB*, Δ*aphB*Δ*chsR*, and Δ*aphB*-OE-*chsR* (Δ*aphB* with a plasmid containing *chsR* with the trc promoter) strains in AKI medium under anaerobic conditions. **e**, qRT–PCR expression levels of *tcpP* in the WT, Δ*fur*, Δ*fur*-OE-*chsR*, and Δ*fur*-OE-*chsR* (Δ*fur* with a plasmid containing *chsR* with the trc promoter) strains in AKI medium under anaerobic conditions. **f**, qRT–PCR expression levels of *tcpP* in the WT, Δ*ohrR*, Δ*ohrR*Δ*chsR*, and Δ*ohrR*-OE-*chsR* (Δ*ohrR* with a plasmid containing *chsR* with the trc promoter) strains in AKI medium under anaerobic conditions (n = 3). Significance was determined by a two-tailed unpaired Student's t test(c-f) and indicated as the P value. *P < 0.05, **P < 0.01, ***P < 0.001; n.s. no significant difference. Data are presented as mean ± s.d. (c-f). Source data are included in the Extended Source Data file.

https://doi.org/10.1038/s41564-024-01823-6

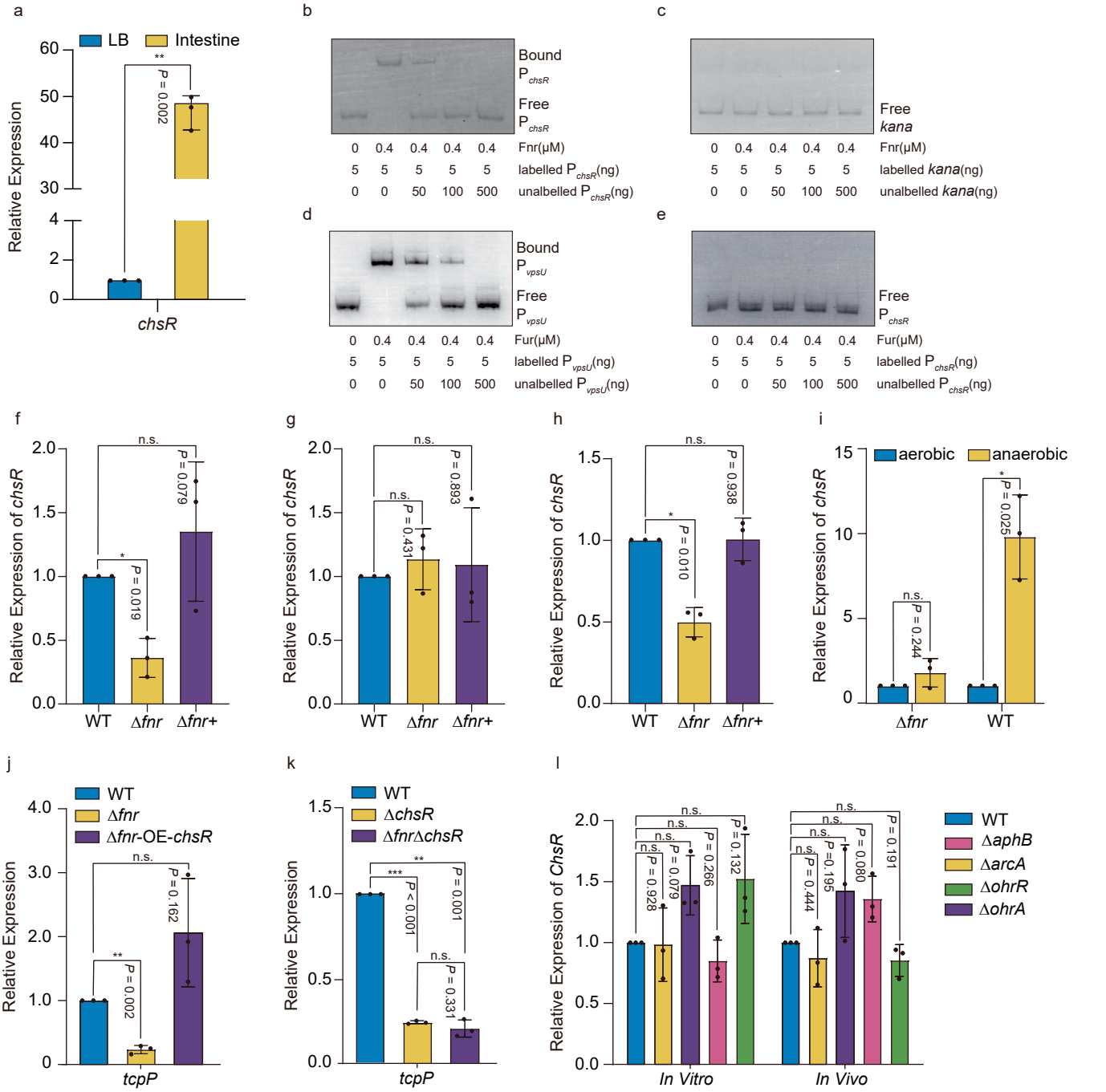

Extended Data Fig. 3 | The ChsR-mediated virulence regulatory pathway is induced by a low O_2 signal in the small intestine of the host via Fnr. **a**, qRT–PCR expression level of *chsR* in the small intestine of mice and LB medium (n = 3). **b**, **c**, Competitive EMSA of the Fnr to FAM-labeled and unlabeled P_{chsR}(b) and *kana* (c, negative control). **d**, **e**, Competitive EMSA of the Fur to FAM-labeled and unlabeled P_{upsU} (d, positive control) and P_{chsR}(e). **f**, **g**, qRT–PCR expression levels of *chsR* in WT, Δ*fnr* and Δ*fnr*+ under anaerobic (f) or aerobic (g) conditions in AKI medium (n = 3). **h**, qRT–PCR expression levels of *chsR* in WT, Δ*fnr* and Δ*fnr*+ in the mouse small intestine (n = 3). **i**, qRT–PCR expression levels of *chsR* in WT and Δ*fnr* under anaerobic or aerobic conditions in AKI medium (n = 3). **j**, qRT–PCR expression levels of *tcpP* in the WT, Δ*fnr*, and Δ*fnr*-OE-*chsR* (Δ*fnr* with a plasmid containing *chsR* with the trc promoter) strains in AKI medium under anaerobic conditions (n = 3). **k**, qRT–PCR expression levels of *tcpP* in the WT, Δ*chsR*, and Δ*fnr*Δ*chsR* strains in AKI medium under anaerobic conditions (n = 3). **l**, qRT–PCR expression levels of *chsR* in WT, Δ*arcA*, Δ*ohrA*, Δ*aphB*, and Δ*ohrR* strains in AKI medium (*In Vitro*) or mouse small intestine (*In Vivo*) (n = 3). Significance was determined by two-tailed unpaired Student's t test (a, f-l) and indicated as the P value. *P < 0.05, **P < 0.01, ***P < 0.001; n.s. no significant difference. Data are presented as mean ± s.d. (f-l). Results are representative of three biological replicate experiments (b-e). Source data are included in the Extended Source Data file.

https://doi.org/10.1038/s41564-024-01823-6

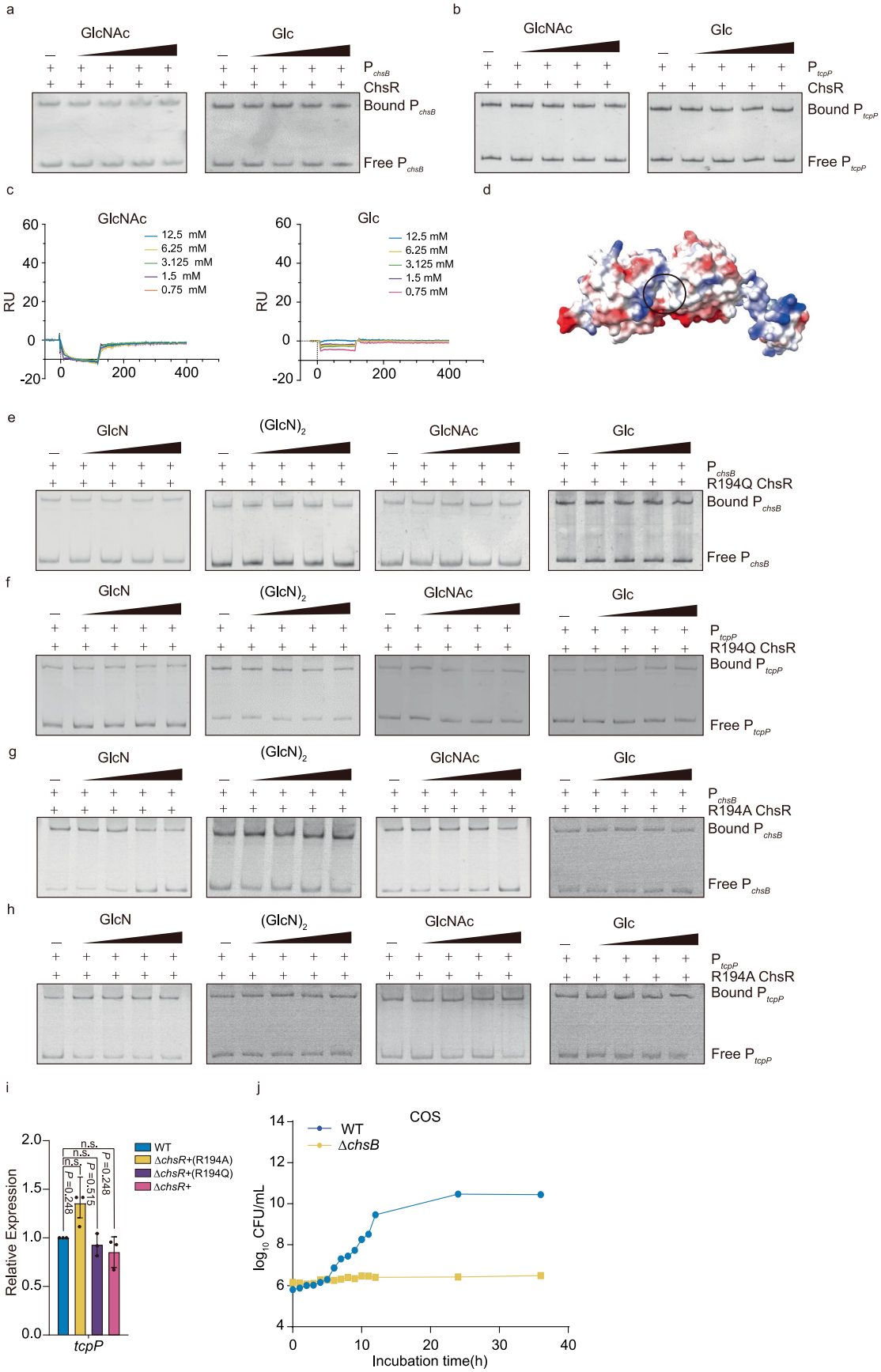

Extended Data Fig. 4 | See next page for caption.

https://doi.org/10.1038/s41564-024-01823-6

Extended Data Fig. 4 | Arg194 in ChsR is indispensable for binding to ligands. **a**, **b**, The influence of GlcNAc and Glc on the binding of purified ChsR protein to the promoter region of *chsB* (a) and *tcpP* (b). **c**. Biacore SPR kinetic analyses of GlcNAc and Glc to ChsR. Sensorgram and saturation curve of the titration of different substrates on ChsR immobilized on a CM5 chip. **d**. Electrostatic properties of ChsR predicted by the AlphaFold Protein Structure Database. Red represents a negative charge, and blue represents a positive charge. The binding pocket is highlighted with a black circle. **e**-**h**, The influence of GlcN, $(GlcN)_2$, GlcNAc and Glc on the binding of purified R194Q ChsR(e, f) or R194A(g, h) ChsR to the promoter region of *chsB*(e, g) and *tcpP*(f, h). **i**, qRT–PCR expression levels of *chsR* in WT, Δ*chsR* + (R194A), Δ*chsR* + (R194Q) and Δ*chsR*+ in AKI medium. **j**, Growth curves of WT and Δ*chsB* in M9 medium containing 0.5% COS as the only carbon source. Significance was determined by a two-tailed unpaired Student's t test and indicated as the P value. *P < 0.05, **P < 0.01, ***P < 0.001; n.s. no significant difference. Data are presented as mean ± s.d. (i, j). Results are representative of three biological replicate experiments (a, b, e-h). Source data are included in the Source Data file.

https://doi.org/10.1038/s41564-024-01823-6

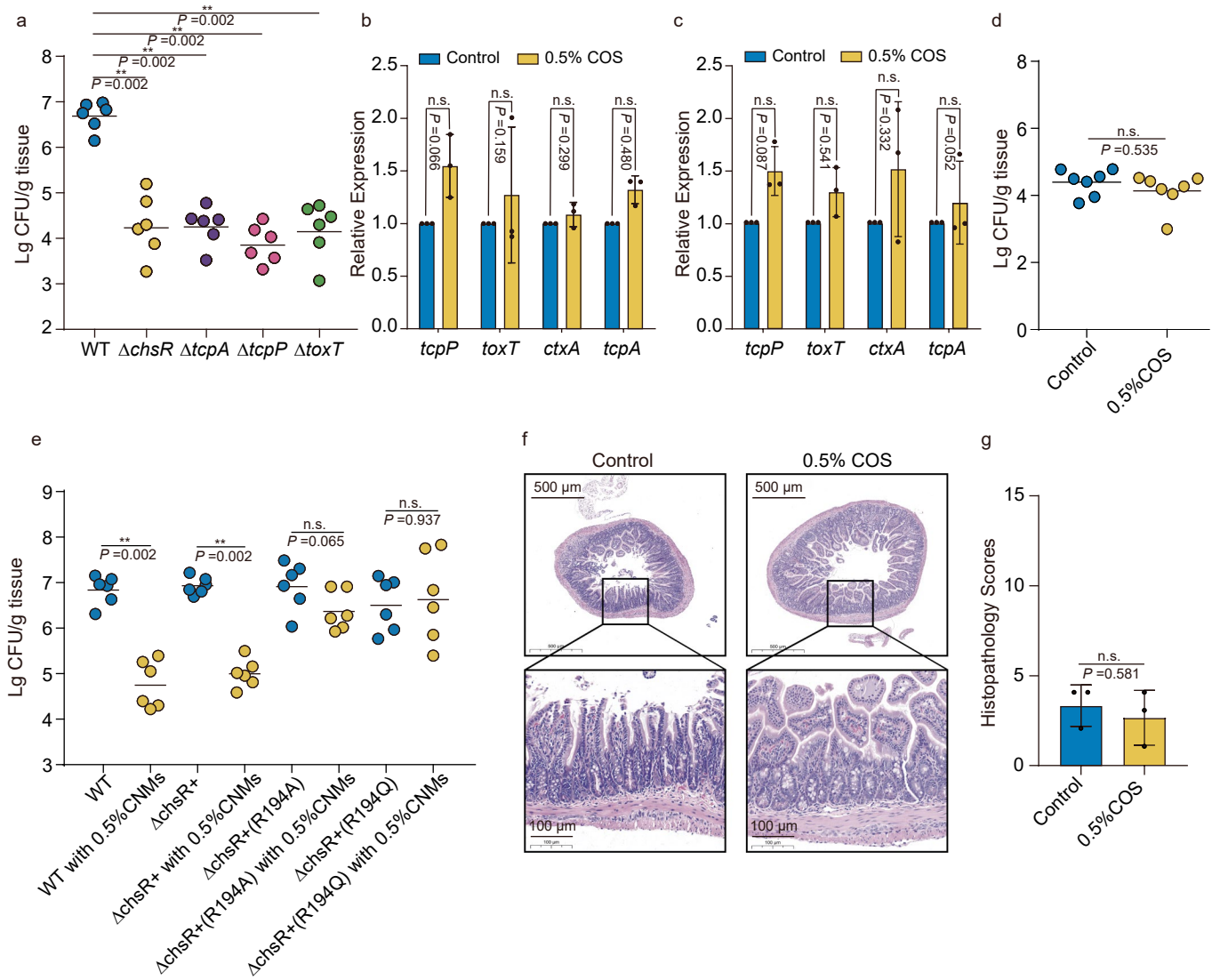

Extended Data Fig. 5 | COS has no effect on the colonization of Δ*chsR* in the small intestine of mice. a, Evaluation of the colonization ability of WT, Δ*chsR*, Δ*tcpA*, Δ*tcpP* and Δ*toxT* in the small intestine of antibiotic cocktail (ampicillin, neomycin, metronidazole, and vancomycin)-treated adult mice (n = 6). **b**, **c**, qRT–PCR expression levels of virulence genes (*tcpP*, *toxT*, *ctxA* and *tcpA*) of Δ*chsR* + (R194Q) (b) or Δ*chsR* + (R194A) (c) in the small intestine of adult mice administered 0.5% COS after 24 h p.i. (n = 3). **d**, Evaluation of the colonization ability of Δ*chsR* in the small intestine of adult mice administered 0.5% COS at the time of bacterial oral challenge (n = 7). **e**, **f**, Representation (e) and histological score (f) of Δ*chsR* in the small intestine of adult mice administered 0.5% COS at the time of bacterial oral challenge (n = 3). **g**, Evaluation of the colonization ability of WT, Δ*chsR* + , Δ*chsR* + (R194A) and Δ*chsR* + (R194Q) in the small intestine of adult mice with or without administration of 0.5% COS at the time of bacterial oral challenge (n = 6). Significance was determined by a two-sided Mann–Whitney U test (a, d, e) or two-tailed unpaired Student's t test (b, c) and indicated as the P value. *P < 0.05, **P < 0.01, ***P < 0.001; n.s. no significant difference. Data are presented as mean ± s.d. (b, c, g). Source data are included in the Source Data file.

https://doi.org/10.1038/s41564-024-01823-6

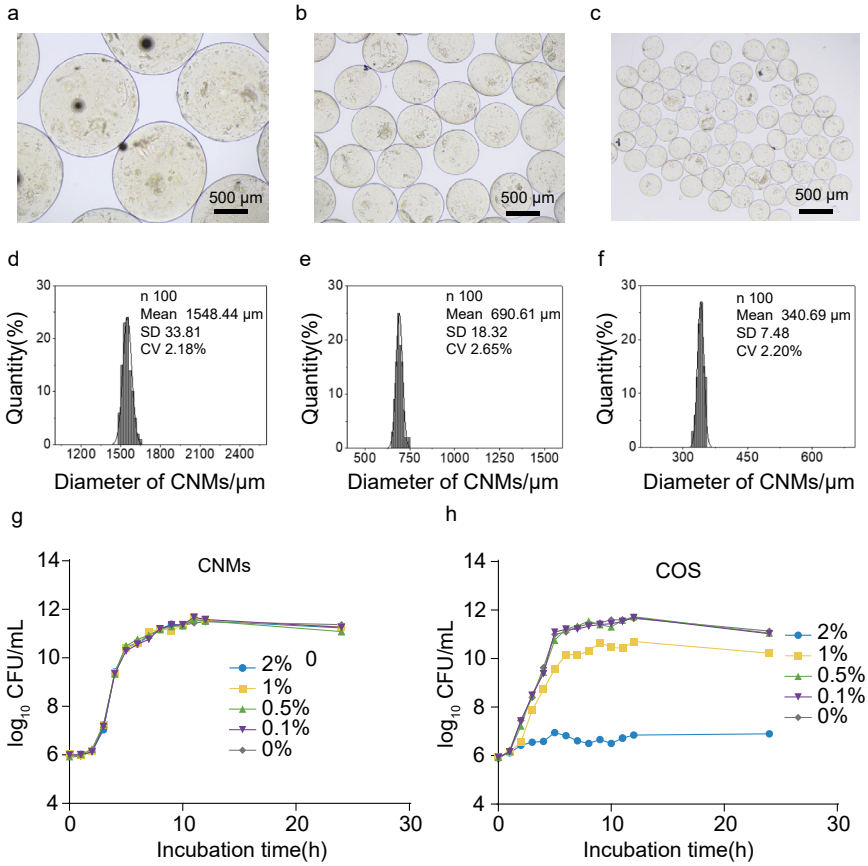

Extended Data Fig. 6 | Controlled generation of microspheres via the gas-shearing method at various nitrogen flow rates. a, **b**, **c**, Bright-field microscopic images of COS NPs@microspheres (CNMs). **d**, **e**, **f**, Quantitative analyses of the diameter distribution of CNMs corresponding to a, b, and c. One hundred microspheres were measured for each map. **g**, **h**, Growth curves of WT in LB medium containing 0-2% CNMs (g) or COS (h). Data are presented as mean ± s.d. (g, h). Results are representative of three biological replicate experiments (a-c). Source data are included in the Source Data file.

https://doi.org/10.1038/s41564-024-01823-6

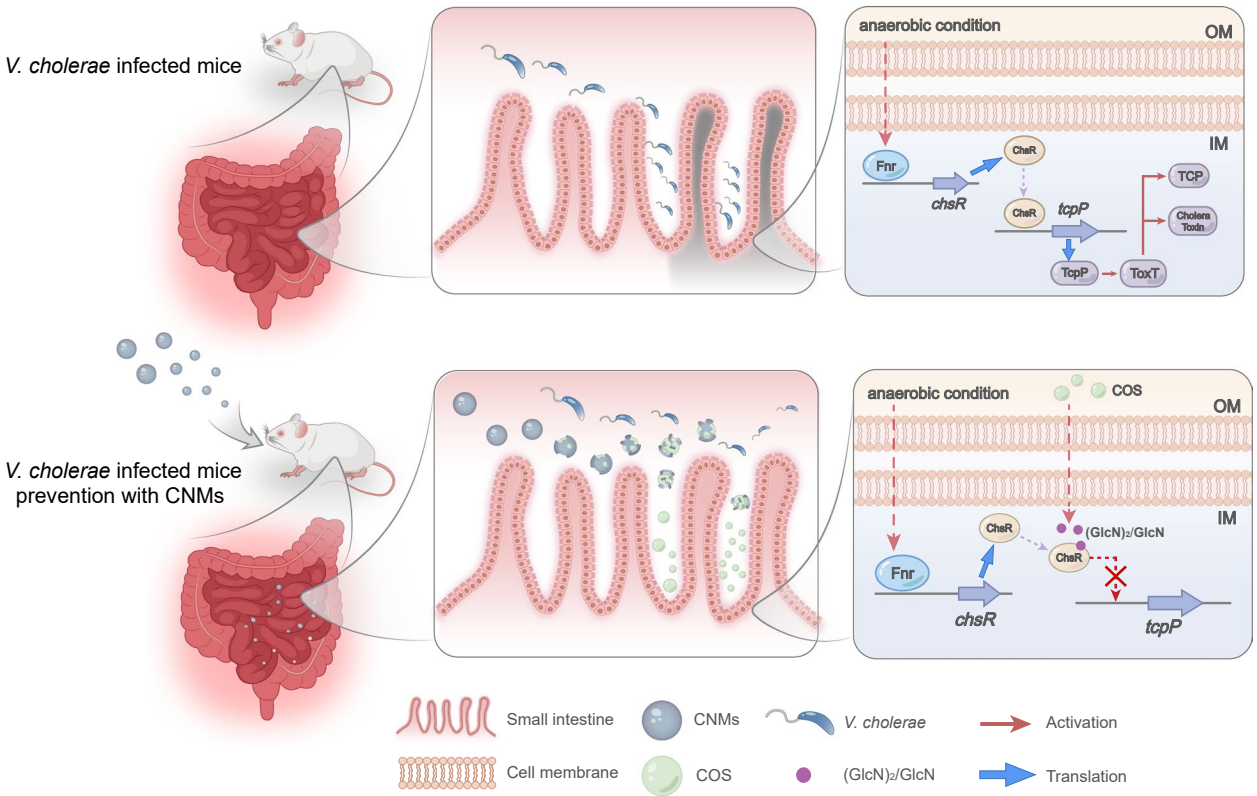

Extended Data Fig. 7 | The schematic illustration of ChsR-mediated regulatory pathway in *V. cholerae* and the utilization of microspheres as COS carriers for the prevention of cholera.

nature portfolio

Corresponding author(s): Bin Liu

Last updated by author(s): Aug 19, 2024

Reporting Summary

Nature Portfolio wishes to improve the reproducibility of the work that we publish. This form provides structure for consistency and transparency in reporting. For further information on Nature Portfolio policies, see our Editorial Policies and the Editorial Policy Checklist.

Statistics

For all statistical analyses, confirm that the following items are present in the figure legend, table legend, main text, or Methods section.

n/a	Confirmed	
☐	☒	The exact sample size (*n*) for each experimental group/condition, given as a discrete number and unit of measurement
☐	☒	A statement on whether measurements were taken from distinct samples or whether the same sample was measured repeatedly
☐	☒	The statistical test(s) used AND whether they are one- or two-sided *Only common tests should be described solely by name; describe more complex techniques in the Methods section.*
☒	☐	A description of all covariates tested
☐	☒	A description of any assumptions or corrections, such as tests of normality and adjustment for multiple comparisons
☐	☒	A full description of the statistical parameters including central tendency (e.g. means) or other basic estimates (e.g. regression coefficient) AND variation (e.g. standard deviation) or associated estimates of uncertainty (e.g. confidence intervals)
☐	☒	For null hypothesis testing, the test statistic (e.g. *F*, *t*, *r*) with confidence intervals, effect sizes, degrees of freedom and *P* value noted *Give P values as exact values whenever suitable.*
☒	☐	For Bayesian analysis, information on the choice of priors and Markov chain Monte Carlo settings
☐	☒	For hierarchical and complex designs, identification of the appropriate level for tests and full reporting of outcomes
☒	☐	Estimates of effect sizes (e.g. Cohen's *d*, Pearson's *r*), indicating how they were calculated

Our web collection on statistics for biologists contains articles on many of the points above.

Software and code

Policy information about availability of computer code

Data collection	Sequencing data was collected by Illumina HiSeq 2500 (Illumina); proteomics data collected by Thermo ScientificTM Q ExactiveTM; Foot-printing data was collected by ABI 3730X; SPR data was collected by Biacore X100.
Data analysis	MedCalc (v12.3.0.0); Microsoft Excel 2019 (16.0.14026.20294); GraphPad Prism(v7.0.4); ImageJ (v1.8.0); DESeq2(v1.12.3); Integrative Genomics Viewer(2.11.3); BWA mem (version 0.7.12); Cutadapt (v1.9.1); MACS2 (v2.1.0); Peak Scanner (v1.0); AutoDockTools (v1.5.6); Biacore X100 evaluation software.

For manuscripts utilizing custom algorithms or software that are central to the research but not yet described in published literature, software must be made available to editors and reviewers. We strongly encourage code deposition in a community repository (e.g. GitHub). See the Nature Portfolio guidelines for submitting code & software for further information.

Data

Policy information about availability of data

All manuscripts must include a data availability statement. This statement should provide the following information, where applicable:

- Accession codes, unique identifiers, or web links for publicly available datasets
- A description of any restrictions on data availability
- For clinical datasets or third party data, please ensure that the statement adheres to our policy

The RNA-seq data have been deposited in the NCBI Sequence Read Archive database under accession code PRJNA900711.

The ChIP-seq data have been deposited in the NCBI Sequence Read Archive database under accession code PRJNA963002.
The proteomics data have been deposited in the iProX (integrated proteome resources) (subproject ID: IPX0008142000).
The PDB file of ChsR was generated using AlphaFold Protein Structure Database (https://www.alphafold.com/search/text/Q9KSH0_VIBCH).

Research involving human participants, their data, or biological material

Policy information about studies with human participants or human data. See also policy information about sex, gender (identity/presentation), and sexual orientation and race, ethnicity and racism.

Reporting on sex and gender	not applicable
Reporting on race, ethnicity, or other socially relevant groupings	not applicable
Population characteristics	not applicable
Recruitment	not applicable
Ethics oversight	not applicable

Note that full information on the approval of the study protocol must also be provided in the manuscript.

Field-specific reporting

Please select the one below that is the best fit for your research. If you are not sure, read the appropriate sections before making your selection.

☒ Life sciences ☐ Behavioural & social sciences ☐ Ecological, evolutionary & environmental sciences

For a reference copy of the document with all sections, see nature.com/documents/nr-reporting-summary-flat.pdf

Life sciences study design

All studies must disclose on these points even when the disclosure is negative.

Sample size	Sample sizes were determined empirically and according to extensive literature on the V. cholerae infection models, and appropriate statistical analyses were performed. Mice colonization experiments were conducted twice with at least 3 mice ($n \geq 3$) in each group, and the combined data for the two experiments was used for statistical analysis. For RNA-seq, the RNA collected from three different biological samples of WT and ΔchsR infected the infant mouse intestine. Three samples were combined for RNA-seq analysis. All other in vitro experiments were repeated at least three times ($n \geq 3$). For immunostaining experiments, three visual fields from each mouse were analyzed, and five mice were examined.
Data exclusions	No data were excluded from the analyses.
Replication	All the reported experiments were reproducible. Data reproducibility was confirmed by three independent experiments. RNA-seq results were validated by three independent qRT-PCR analyses on target genes.ChIP-seq results were validated by three independent ChIP-qPCR analyses on target peaks. In vitro data used at least 3 biological samples and 3 technical replicates in at least three independent experiments.
Randomization	All samples were assigned to groups randomly. All mice were randomized to avoid cage effects. Other data collection was not randomized, but always done in parallel with controls.
Blinding	cDNA ibraries were constructed and analyzed by Majorbio, Inc. (Shanghai, China), which also provided the statistical analysis. ChIP-seq libraries were constructed and analyzed by NOVOGENE, Inc (TianJin, China), which also provided the statistical analysis. Most experiments were conducted by at least two different researchers who have not known the situation and results of the study in advance and repeated on at least two independent days. The stained sections were blindly scored for inflammation severity.

Reporting for specific materials, systems and methods

We require information from authors about some types of materials, experimental systems and methods used in many studies. Here, indicate whether each material, system or method listed is relevant to your study. If you are not sure if a list item applies to your research, read the appropriate section before selecting a response.

Materials & experimental systems

n/a	Involved in the study
☐	☒ Antibodies
☒	☐ Eukaryotic cell lines
☒	☐ Palaeontology and archaeology
☐	☒ Animals and other organisms
☒	☐ Clinical data
☒	☐ Dual use research of concern
☒	☐ Plants

Methods

n/a	Involved in the study
☐	☒ ChIP-seq
☒	☐ Flow cytometry
☒	☐ MRI-based neuroimaging

Antibodies

Antibodies used

supplier name: abcam, catalog number: ab191598, clone name: Anti-RNA polymerase beta antibody, lot number: 1000526-3, dilution:1:2000
supplier name: abcam, catalog number: ab123129, clone name: Anti-Cholera Toxin antibody; lot number: GR3254532-14, dilution:1:2000
supplier name: sigma, catalog number: F1804, clone name: Monoclonal ANTI-FLAG® M2 antibody, dilution:1:1000
supplier name: Sparkjade, catalog number: EF0002, clone name: HRP-conjugated goat anti-rabbit IgG secondary antibody; lot number: WADCQ, dilution:1:1000

Validation

Anti-RNA polymerase beta antibody : Rabbit monoclonal to RNA polymerase beta; Suitable for: IP, WB; Reacts with: Escherichia coli.
Anti-cholera toxin antibody: Rabbit polyclonal to Cholera Toxin; Suitable for: WB, ELISA; Reacts with: Vibrio cholerae.
Monoclonal ANTI-FLAG® M2 antibody: Produced in mouse; species reactivity: all.
Resuts using these antibody were previously published(Nat Commun. 2021; 12: 4649.; Proc Natl Acad Sci U S A . 2022 Nov 29;119(48):e2212436119.; Commun Biol. 2022 Jun 8;5(1):559. ; Gut Microbes . 2022 Jan-Dec;14(1):2143216.)

Animals and other research organisms

Policy information about studies involving animals; ARRIVE guidelines recommended for reporting animal research, and Sex and Gender in Research

Laboratory animals	5-days-old CD-1 infant mice; Six-week-old specific-pathogen-free BALB/c mice
Wild animals	This study did not involve wild animals.
Reporting on sex	Both sexes of CD-1 infant mice; female specific-pathogen-free BALB/c mice
Field-collected samples	This study did not involve samples collected from the field.
Ethics oversight	All animal studies were conducted according to protocols approved by the Institutional Animal Care Committee of Nankai University (Tianjin, China) and performed under protocol no. IACUC 2016030502.

Note that full information on the approval of the study protocol must also be provided in the manuscript.

Plants

Seed stocks	This study did not involve plants.
Novel plant genotypes	not applicable
Authentication	not applicable

ChIP-seq

Data deposition

☒ Confirm that both raw and final processed data have been deposited in a public database such as GEO.

☒ Confirm that you have deposited or provided access to graph files (e.g. BED files) for the called peaks.

Data access links *May remain private before publication.*	https://www.ncbi.nlm.nih.gov/bioproject/PRJNA963002
Files in database submission	vc1286input_1.fq(mock-ChIP); vc1286input_2.fq(mock-ChIP); vc1286chip_output_1(ChsR-ChIP);

Files in database submission	vc1286chip_output_2.fq(ChsR-ChIP)
Genome browser session (e.g. UCSC)	https://www.ncbi.nlm.nih.gov/assembly/GCF_007624355.1

Methodology

Replicates	ChIP-seq was performed once for the ChIP sample (ChsR-ChIP) and the mock ChIP sample (mock-ChIP). The promoter region of tcpP and chsB were significantly enriched in the ChIP sample compared to that in the mock ChIP sample. The ChIP-qPCR results (from three independent biological experiments) confirmed the enrichment of the tcpP and chsB promoter region in the ChIP sample.
Sequencing depth	Sequencing layout: 2×150 paired-end Sequencing Depth for each sample (ID: total number of reads/uniquely mapped) mock-ChIP:15207692/14501059(98.02%) ChsR-ChIP:15828526/13951938(96.39%)
Antibodies	Anti-FLAG mouse monoclonal antibody (Sigma #F1804)
Peak calling parameters	Peaks were called using MACS2 with default settings and the fragment size set to 150 bp (option '--extsize 150').
Data quality	Only uniquely mapped reads with an alignment score ≥ 20 were used for peak calling. After mapping reads to the reference genome, the MACS2 (v2.1.0) peak finding algorithm was used to identify regions of IP enrichment over control. A q value threshold of enrichment of 0.05 was used for all data sets.
Software	Quality control: Cutadapt (v1.9.1) Read mapping: BWA mem (v0.7.12) Peak calling: MACS2 (v2.1.0) Visual analysis:Integrative Genomics Viewer(2.11.3)